PNAS
www.pnas.org

Supplementary Information for

Membraneless Polyester Microdroplets as Primordial Compartments at the Origins of Life

Tony Z. Jia, Kuhan Chandru, Yayoi Hongo, Rehana Afrin, Tomohiro Usui, Kunihiro Myojo, H. James Cleaves II

Corresponding Author: Tony Z. Jia
Email: tzjia@elsi.jp

Corresponding Author: Kuhan Chandru
Email: kuhan@ukm.edu.my

This PDF file includes:

Supplementary Methods
Figs. S1 to S37
Scheme S1
Tables S1 to S7
Captions for Movies S1 to S12
References for SI reference citations

Other supplementary materials for this manuscript include the following:

Movies S1 to S12

www.pnas.org/cgi/doi/10.1073/pnas.1902336116

Table of Contents

Supplementary Methods	3
Supplementary Figures	13
Supplementary Scheme	50
Supplementary Tables	51
Supplementary Movies	68
References	69

Supplementary Methods

Chemicals. DL-Leucic Acid (DL-2-Hydroxy-4-methylpentanoic acid, MA) and 2-hydroxy-4-(methylsulfanyl)butanoic acid (SA) were purchased from Tokyo Chemical Industry Co. (Chuo-ku, Tokyo, Japan). SYBR Gold, Rhodamine-PE (Lissamine™ Rhodamine B 1,2-dihexadecanoyl-*sn*-glycero-3-phosphoethanolamine, triethylammonium salt), and 2X Novex TBE-Urea Sample Buffer was purchased from Thermo-Fisher Scientific (Minato-ku, Tokyo, Japan). MES (2-(N-morpholino)ethanesulfonic acid) was purchased from Dojindo Molecular Technologies (Kamimashiki-gun, Kumamoto, Japan). Glycogen was purchased from Fujifilm Wako Pure Chemical Industries (Osaka, Osaka-fu, Japan). Urea was purchased from Nacalai Tesque, Inc. (Kyoto, Kyoto-fu, Japan). RNA was purchased from Integrated DNA Technologies (Minato-ku, Tokyo, Japan) and used without further purification. All other reagents including glycolic acid (GA), DL-lactic acid (LA), and DL-3-phenyllactic acid (PA) were purchased from Sigma-Aldrich (Chuo-ku, Tokyo, Japan) unless otherwise noted.

Synthesis of Polyesters. All experiments were conducted in open borosilicate test tubes unless otherwise noted. pH was not adjusted, resulting in starting pHs of roughly 1.5–3 (LA: pH 1.5–2, GA: pH 2–2.5, PA: pH 2.5, SA: pH 3, MA: pH 2–2.5, all five αHAs mixed sample: pH 2–2.5) as measured using Sigma-Aldrich Hydrion Brilliant disposable pH sticks, which are accurate to ± 0.5 pH unit. Reactions performed at pH 7 (*SI Appendix* Fig. S4) were unbuffered; the pH of the solutions was brought to pH 7 by addition of aqueous NaOH (1 or 5N). Reactions were held at constant temperature (± 0.1°C) using Sahara 310 dry heating baths (Rocker Scientific, New Taipei City, Republic of China). Starting total concentrations of all reactions were 500 mM αHA in ultrapure water with a resistance of 22.2 MΩ•cm (Millipore Q-UV5 system, Burlington, Massachusetts, USA). For example, individual αHA reactions contained were 500 mM of a single αHA, while a 5 αHA mixed reaction contained 100 mM of each αHA (for a total of 500 mM total αHA concentration). These samples were allowed to dry at 80°C for 1 week. Conditions such as temperature, time, or pH (adjusted using aqueous NaOH) were also varied. All further experiments used ultrapure or molecular biology-grade water (GE Healthcare HyClone,

Hino-shi, Tokyo, Japan). All macroscopic condensed phase photographs (*e.g.*, non-microscopic images) were taken with an iPhone 6 or an iPhone SE (Cupertino, California, USA).

Matrix Assisted Laser Desorption Ionization Mass Spectrometry (MALDI-MS). MALDI-MS spectra were acquired using an ultrafleXtreme Brucker Daltonics MALDI-TOF-MS in positive ion mode. External mass calibration was conducted using standard peptide mixtures (Brucker Daltronics). Sample preparation matrices (trans-2-[3-(4-tert-butylphenyl)-2-methyl-2- propenylidene]malononitrile (DCTB) or dithranol) were dissolved in tetrahydrofuran (THF) (10 mg/mL). For polyGA, because the synthesis product was not soluble in THF, 1 μL of the sample dissolved in acetonitrile was applied to the plate and dried, and then 1 μL of the dithranol matrix was added to the dried sample. After drying again, the sample was analyzed by MS. For the other four single αHA samples, the samples and the matrix (DCTB) were mixed at a 1:10 (v/v) ratio in advance and then the mixture was applied to the plate before analysis.

Peaks were compiled and identified (Tables S1–S5) by isolating the highest intensity peak in an isotope envelope that corresponded to a polymer product using a peak list generated from mMass (Open Source Software, Prague, Czech Republic) after baselining and thresholding above an intensity of 100 (or in the case of polySA, an intensity of 500 due to the noisy baseline). The monoisotopic mass peak is reported. Mass accuracy (in ppm) was calculated by comparing the observed mass with the calculated mass. Analytical settings, matrix, and thresholding parameters were identical among different runs of experiments using different monomers. Although we also found other adducts, such as M+K, we list only M+Na and M+2Na-H peaks, which are the adducts that most clearly show mass ladders.

For Figure S3, dithranol was used as the matrix for unpolymerized GA, SDHB (mixture of 2,5-dihydroxybenzoic acid and 2-hydroxy-5-methoxybenzoic acid) was used as the matrix for unpolymerized LA and SA, and DCTB (trans-2-[3-(4-tert-butylphenyl)-2-methyl-2-propenylidene]malononitrile) was used as the matrix for unpolymerized PA and

MA. Each sample was dissolved to be around 10 mg/mL (LA and SA in water, and GA, PA, and MA in THF). For GA, PA, and MA, 1μL of the sample (dissolved in THF) was applied to the plate and dried, and then 1 μL of the respective matrices was added to the dried sample. After drying again, the samples were analyzed by MS. For LA and SA, the samples and the matrix (SDHB) were mixed at a 1:10 (v/v) ratio in advance and then the mixture was applied to the plate before analysis.

Optical Microscopy. All droplet experiments began with dried polyester being freshly hydrated in 500 μL 4:1 (v/v) water:acetonitrile (unless otherwise noted), followed by brief sonication and vortexing. The pH after dissolution was always in the range of 2–3. Acetonitrile was incorporated into the medium to assist in detaching the condensed phase from the glass surface and the formation of droplets; in the absence of acetonitrile, when only using water, the condensed phase remained at the bottom of the glass tube even with vigorous continuous vortexing and/or sonication and formed no droplets, while in other cases, very few droplets formed (Fig. S7). Immediately after vortexing, 3.5–5 μL of the sample was applied to a glass coverslip (No. 1 22 x 32 mm, Matsunami Glass, Kishiwada-shi, Osaka, Japan) into a vacated area within a double-sided tape ring. This was then covered by a second glass coverslip of the same size. Optical microscopy images were acquired with an Olympus (Shinjuku-ku, Tokyo, Japan) IX73 inverted fluorescent microscope on a 40 x 0.60 air Ph2 LUCPlanFL objective. All images were analyzed using FIJI (Fiji is Just ImageJ, http://fiji.sc). Observations were performed in duplicate or greater.

For optical microscopy experiments assessing temperature stability (Fig. S24), each sample (microdroplets in 4:1 v/v water/acetonitrile) was transferred to 2 mL plastic Eppendorf tubes, then heated up to 90°C using a dry bath, and allowed to incubate for at least 5 min. The sample was then cooled to room temperature in the Eppendorf tube, and the sample slide was prepared and then imaged as described above.

For experiments involving dilution (Figs. S14–S15 and Movies S1–S2), droplets were diluted 1:10 in milliQ water (final water:acetonitrile ratio of 49:1 (v/v)), and then

immediately applied to the glass coverslip and observed for several hours. If the droplets were diffusing over time, then the viewing window was manually adjusted as needed so that the droplet being tracked was always in the viewing window.

For the experiments examining pH stability (Figs. S17–S21, Movies S5–S6), each sample was directly dissolved in 400 µL 1M Na-HEPES pH 8 followed by addition of 100 µL acetonitrile for a final Na-HEPES concentration of 800 mM (and a final water:acetonitrile ratio of 4:1 (v/v)). For samples after incubation for 24 hours (Fig. S18), the sample was prepared identical to that described immediately above, and visualized after vortexing. For the experiments involving salt stability (Figs. S22–S23, Movies S7–S9), each sample was first dissolved in 4:1 (v/v) water:acetonitrile, and then a stock solution of 1 M NaCl or 1 M Na-HEPES pH 8 was added to the solution to a final concentration of 100 mM NaCl or 100 mM Na-HEPES pH 8 (for a final water:acetonitrile ratio of 84:16 (v/v)). The samples were then prepared at the specific time point stated for imaging as described above.

Particle Size Image Analysis. For image analysis using FIJI, default thresholding was used, in addition to the "Analyze Particles" function with **Size = (1.05 – infinity)** and **Circularity = 0.00 – 1.00**, while excluding any particles "detected" that reside on the edge of the image (except in the case of the polyMA sample heated to 90°C, where there was clearly one large particle that would not have been counted properly), particles which were smaller than 10 pixels (Area = 0.104–1.041 square µm), and large areas which were clearly not particles (which are all caused by patches of heterogeneous background intensity typically at the edges of the image that were incorrectly identified as particles). We assumed that all particles were spheres, and thus back-calculated the diameter of each particle from its computed area.

Fluorescence Microscopy. Each dried polyester was dissolved in 500 µL 4:1 v/v water:acetonitrile and sonicated and vortexed briefly. Then, to these samples, concentrated solutions (100 µM) of fluorescent RNA (5′-FAM-CGCGCCGAAACACCGUGUCUCGAGC-3′) (6-carboxyflouorescein = FAM), SYBR

Gold (10X), or thioflavin T (TfT, 200 mM) were added to a final concentration of 10 μM RNA, 1X SYBR Gold, or 20 mM TfT (for a final water:acetonitrile ratio of 82:18 (v/v)). For the 3.5–5 μL of the sample was then applied to a glass coverslip (No. 1 22 x 32 mm, Matsunami Glass, Kishiwada-shi, Osaka, Japan) into a vacated area within a double-sided tape ring. This was then covered by a second glass coverslip of the same size. For imaging of sfGFP (superfold GFP) in polyPA droplets (Fig. S33), 8 μL of a polyPA droplet suspension in 4:1 (v/v) water:acetonitrile was prepared. To this, 2μL of concentrated MES (2-(N-morpholino)ethanesulfonic acid) pH 5.7 (1M) was added to a final buffer concentration of 200 mM MES pH 5.7. Then, 2μL of a a 1:16-fold dilution (in 200 mM MES pH 5.7) of sfGFP after *in vitro* synthesis and purification (*vide infra*) was added to 10 μL of the polyPA droplet suspension (already in 200 mM MES pH 5.7) (for a final water:acetonitrile ratio of 13:2 (v/v)) and then the microscope sample procedures above were followed.

For experiments tracking RNA localization to polyPA over time (Fig. S36), we prepared a 30 or 50 μL solution of 10 μM HH1 (5′-FAM-CGCGCCGAAACACCGUGUCUCGAGC-3′), 200 mM MES pH 5.7, and 100 mM $MgCl_2$. After 8 hours of incubation at room temperature, we slightly mixed the sample by vortex, and then prepared the sample slides and imaged the sample as described above.

For confocal imaging of microdroplets with Rhodamine-PE (Lissamine™ Rhodamine B 1,2-dihexadecanoyl-*sn*-glycero-3-phosphoethanolamine, triethylammonium salt), 3 μL of a 20 μM stock solution of Rhodamine-PE and 6 μL of 2M MES pH 5.7 was added to 21 μL of a polyPA droplet suspension in 4:1 (v/v) water:acetonitrile, to a final concentration of 2 μM Rhodamine-PE and 200 mM MES pH 5.7 (for a final water:acetonitrile ratio of 86:14 (v/v)). 25 μL of this sample was then added to the interior of a Frame-Seal™ 25μL incubation chamber (Bio-Rad, Hercules, California, USA) mounted on a glass cover slide (same as above) and then sealed with another glass cover slide. Epifluorescence microscopy images were acquired with an Olympus (Shinjuku-ku, Tokyo, Japan) IX73 inverted fluorescent microscope on a 40X 0.60 air Ph2 LUCPlanFL N objective with blue (436 nm) or green (546 nm) laser excitation (U-HGLGPS light guide-coupled

illumination system). Figure S36 was acquired on the same microscope but on a 100X 1.30 Oil Ph3 UPlanFL N objective. Fluorescence recovery after photobleaching (FRAP) experiments were performed with unadjusted-pH samples with an Olympus IX81 confocal microscope using a 20X 0.75 air UPlanSapo objective with 473 nm (TfT, SYBR Gold, and fluorescent RNA) or 559 nm (Rhodamine-PE) excitation and FITC (TfT, SYBR Gold, and fluorescent RNA) or Cy3 (Rhodamine-PE) emission channels. Images were analyzed using FIJI. FRAP data was acquired for at least three droplets per sample.

FRAP analyses were carried out according to the method of Phair, et al. (34). We can qualitatively compare compartmentalization by the length of time required for a bleached sample to recover its fluorescence; shorter recovery times imply more exchange between the interior of the droplet and the surrounding medium (*i.e.*, less stable compartmentalization), while longer recovery times imply little exchange between the droplet interior and the surrounding medium (more stable compartmentalization). Using FIJI, the average intensity of the bleached droplet ($\mathbf{A_t}$), the average intensity of an unbleached droplet away from the bleaching site (a control which is unaffected by the bleaching process ($\mathbf{C_t}$), and the average intensity of a background area devoid of fluorescence intensity ($\mathbf{B_t}$) were obtained at each timepoint **t** as well as before bleaching ($\mathbf{A_0}$, $\mathbf{C_0}$, and $\mathbf{B_0}$, respectively). The normalized intensity at time **t** (**I(t)**) was calculated as follows:

$$I(t) = \frac{\left(\frac{A_t - B_t}{C_t - B_t}\right)}{\left(\frac{A_0 - B_0}{C_0 - B_0}\right)}$$

Recovery kinetics were fit using OriginLab (Northampton, MA), assuming single exponential recovery kinetics (given the sphericality of the droplets) using the following equation:

$$I = I_0 + Ae^{\frac{-t}{\tau}}$$

I = fluorescence intensity at time = t, $\mathbf{I_0}$ = intensity at time zero, t = time, A = a constant, and $\boldsymbol{\tau}$ = recovery time constant. $\mathbf{t_{1/2}}$, the half-time of recovery, was calculated as Ln(2)*$\boldsymbol{\tau}$. Please see Table S6.

Spatial Fluorescence Dispersion Kymograph Analysis. We utilized initial confocal fluorescence images acquired for use in the droplet FRAP assays for TfT and SYBR Gold and arbitrarily selected four droplets within each image. For these droplets, we assumed perfect radial symmetry, and with FIJI, we drew a line along an arbitrary radial axis and generated a kymograph (Figs. S26–S30).

Functional Ribozyme Assays. The hammerhead ribozyme reaction was performed in the following conditions: 4 μM HH1 (5′-FAM-CGCGCCGAAACACCGUGUCUCGAGC-3′), 6 μM HH2 (5′-GGCUCGACUGAUGAGGCGCG-3′), 200 mM MES pH 5.7, and 100 mM $MgCl_2$ in the presence or absence of polyPA droplets in a total volume of 30 μL. When polyPA droplets were added, the droplet solution after addition of 500 μL 4:1 (v/v) water:acetonitrile was diluted by the other components to a final fraction of 60% of original (the final water:acetonitrile ratio was subsequently 88:12 (v/v)), otherwise in the absence of polyPA, the reaction occurred in pure water. The reaction was assayed up to 24 hours with timepoints taken at 1–2 hour intervals (up to 8 hours) by removing 4.5 μL of each reaction and depositing it into a 200 μL solution of 4:1 ethanol:RNAse-free water, 50 μg/mL glycogen and 125 mM ammonium acetate and leaving it to incubate overnight at –20 °C. A 24 hour timepoint was also taken, and deposited into the same precipitation solution at –20 °C for at least 15 minutes. Then, all samples were centrifuged at 21,500 g for 15 minutes at 4 °C in a himac CT 15RE benchtop centrifuge (Hitachi, Chiyoda-ku, Tokyo, Japan) and the supernatant was removed by pipet. The precipitation and washing step removes unwanted ions and other materials that may interfere with gel electrophoresis analysis. The pellet was dissolved in 5 μL of either 8M Urea in 1X Tris/Borate/EDTA buffer or 2X Novex TBE-Urea Sample Buffer (Thermo-

Fisher Scientific) followed by vigorous pipetting. 2.5 µL of each sample was loaded onto pre-cast 12-well 6% Novex TBE-Urea gels and electrophoresis was performed in a Novex gel running box (Thermo-Fisher Scientific) for 35 minutes at 150V. The gel was then removed from the plastic casing and imaged on an Amersham Imager 600 (GE Life Sciences, Shinjuku-ku, Tokyo, Japan) with the Blue (460 nm) channel on automatic mode.

The resulting gel band intensities were calculated by the software on the imager with Minimum Profile background subtraction. The band intensities were then used to calculate the reaction rate in the following manner. The negative of the log of the intensity of the reactant band (before self-cleavage) as a fraction of the total intensity of both bands was plotted against time in hours, and a linear regression was performed with the linear range of the plot (first five points up to 8 hours). The observed first order rate constant, k, in h^{-1} is the slope of the regression fit (Figs. S34–S35).

All buffers used in this section were either made with RNAse-free water and subsequently filtered, or were purchased as RNAse free (except the sample loading buffer purchased from Thermo-Fisher).

Heterologous expression and purification of superfold green fluorescent protein (sfGFP). The gene encoding sfGFP (RCSB PDB 2B3P) with an N-terminal 6His tag was synthesized and cloned into a pETduet-1 plasmid by Genscript (Chiyoda-ku, Tokyo, Japan). Recombinant sfGFP was affinity purified using Ni Sepharose™ High Performance HisTrap™ (GE Healthcare, Chicago, Illinois, USA) following the standard protocol provided by manufacturer. Briefly, *E. coli* strain NiCo21(DE3) (New England Biolabs, Inc., Ipswich, Massachusetts, USA) carrying the sfGFP expression plasmid was grown in 1 L of Terrific Broth (TB) medium broth with 100 µg/mL ampicillin (Fujifilm Wako Pure Chemical Industries, Osaka, Osaka-fu, Japan) at 37 °C and 200 rpm until an OD600 nm of 0.6 was reached. Protein overexpression was induced with 0.4 mM isopropyl β-D-1-thiogalactopyranoside (IPTG) (Fujifilm Wako Pure Chemical Industries), and the culture was cultivated overnight at 16°C while rotating at 200 rpm.

Cells were collected by centrifugation at 9,000 x g for 15 min, re-suspended in 50 mM HEPES-K^+ buffer (pH 7.5) containing 300 mM NaCl, 5% glycerol (v/v), and 5 mM imidazole (all Sigma-Aldrich, Chuo-ku, Tokyo, Japan). Cells were lysed by pulse-mode sonication on ice for 45 min (3 s on and 4 s off). The lysate was centrifuged at 38,000 x g for 20 min and the supernatant was passed through a column packed with 1 mL of Ni Sepharose™ 80% slurry. After washing with 100 mL of the same buffer, but with a higher imidazole concentration (25 mM), proteins were eluted with 3 mL of this buffer supplemented with 250 mM imidazole, and was desalted using the Amicon Ultra-0.5 mL centrifugal filter (Millipore, Burlington, Massachusetts, USA). Protein concentrations were estimated using the standard Bradford assay (Bio-Rad Laboratories, Hercules, California, USA) and protein purity was examined by 10% SDS-PAGE (Novex®, Thermo Fisher Scientific, Waltham, Massachusetts, USA) and coomassie blue staining (Sigma-Aldrich) (Figure at right). The protein concentration was estimated using a standard Bradford assay (Sigma-Aldrich) to be ~4 mg/mL. The protein stock solutions were flash frozen with liquid nitrogen and stored at -80°C. The N-terminal 6His tag was retained for all experiments.

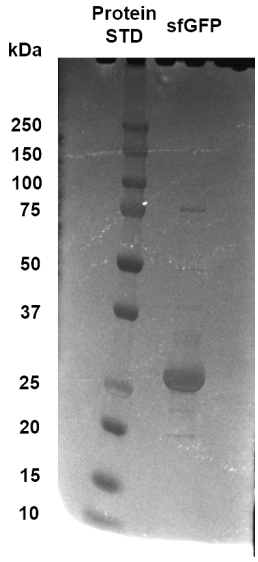

Swelling Assays

500 µL of 500 µM LA and PA were dried in 1.5 mL eppendorf tubes for 3 days at 80°C. After drying, a gel-like material formed. The mass of the sample tube including the gel was acquired, as well as a tube with no sample (each was performed in least triplicate). 500 µL of ultrapure water (22.2 MΩ•cm resistance, Millipore Q-UV5 system, Burlington, Massachusetts, USA) was added to the top of the samples and allowed to incubate at room temperature for 3 days. 500 µL of water was also added to an empty tube and allowed to incubate at room temperature for 3 days. The tubes were then

centrifuged at 21,500 g for 5 minutes. The supernatant (water) was removed by pipetting, and the mass of the sample tube with gel after centrifugation was acquired, as well as the mass of the control tube with no sample; we removed as much of the water as possible by pipet without disrupting the gel phase. These data are presented in Supplementary Table S7.

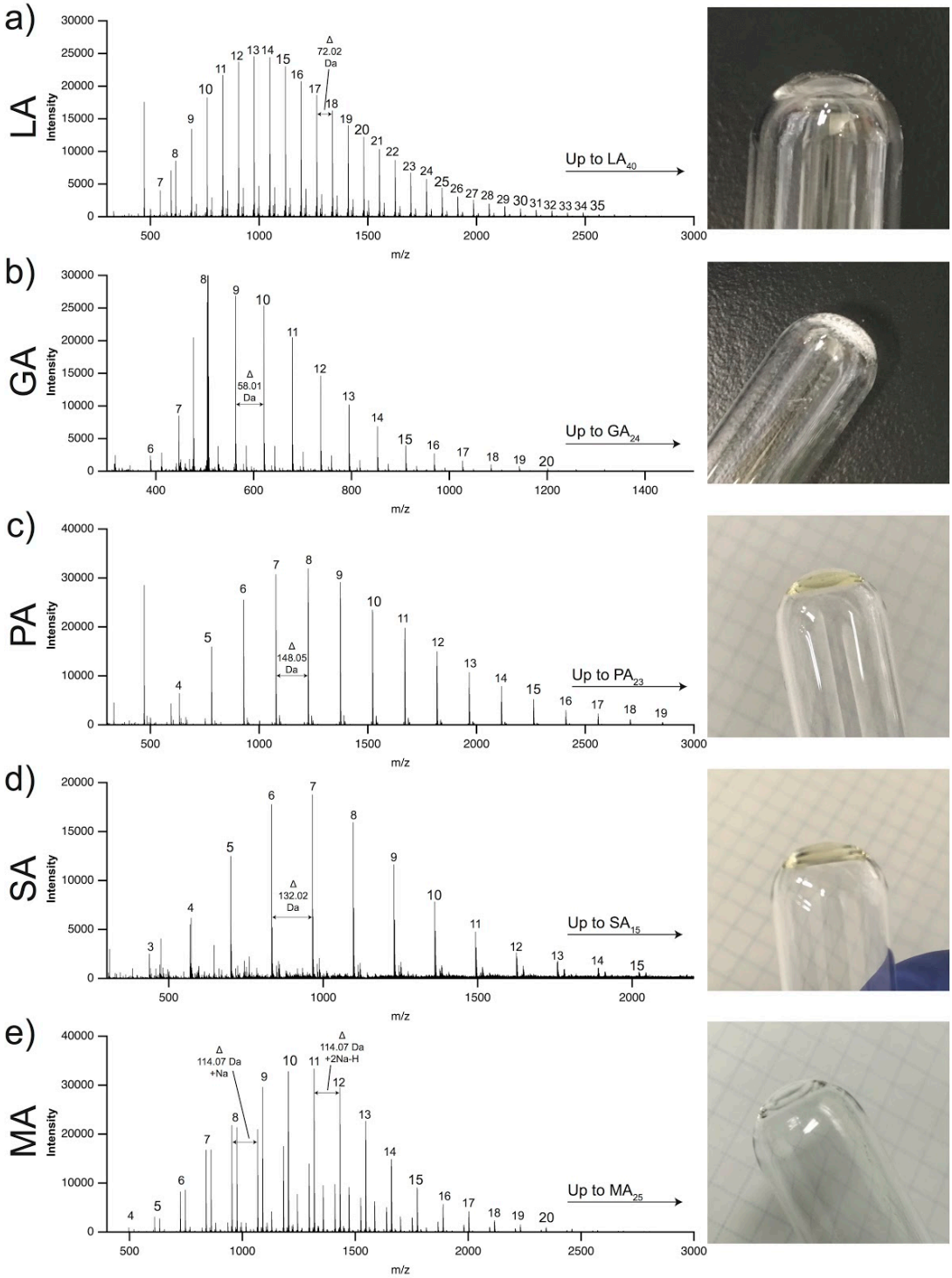

Supplementary Figure S1. Positive ion mode MALDI-TOF mass spectra of polymerization of each αHA (500 mM initial concentration) via drying. Mass increment for **(a)** LA = Δ72.02 Da, **(b)** GA = Δ58.01 Da, **(c)** PA = Δ148.05 Da, **(d)** SA = Δ132.02 Da, **(e)** MA = Δ114.07 Da. Peak labels on spectra indicate the polymer length. All peaks labeled are sodiated adducts (For polyMA, +2Na –H adducts dominate at high mass; both +2Na –H and Na+ adduct peaks are labeled). See Figs. S2–S3 and Tables S1–S5. Accompanying photos show the condensed gel-like phase after synthesis.

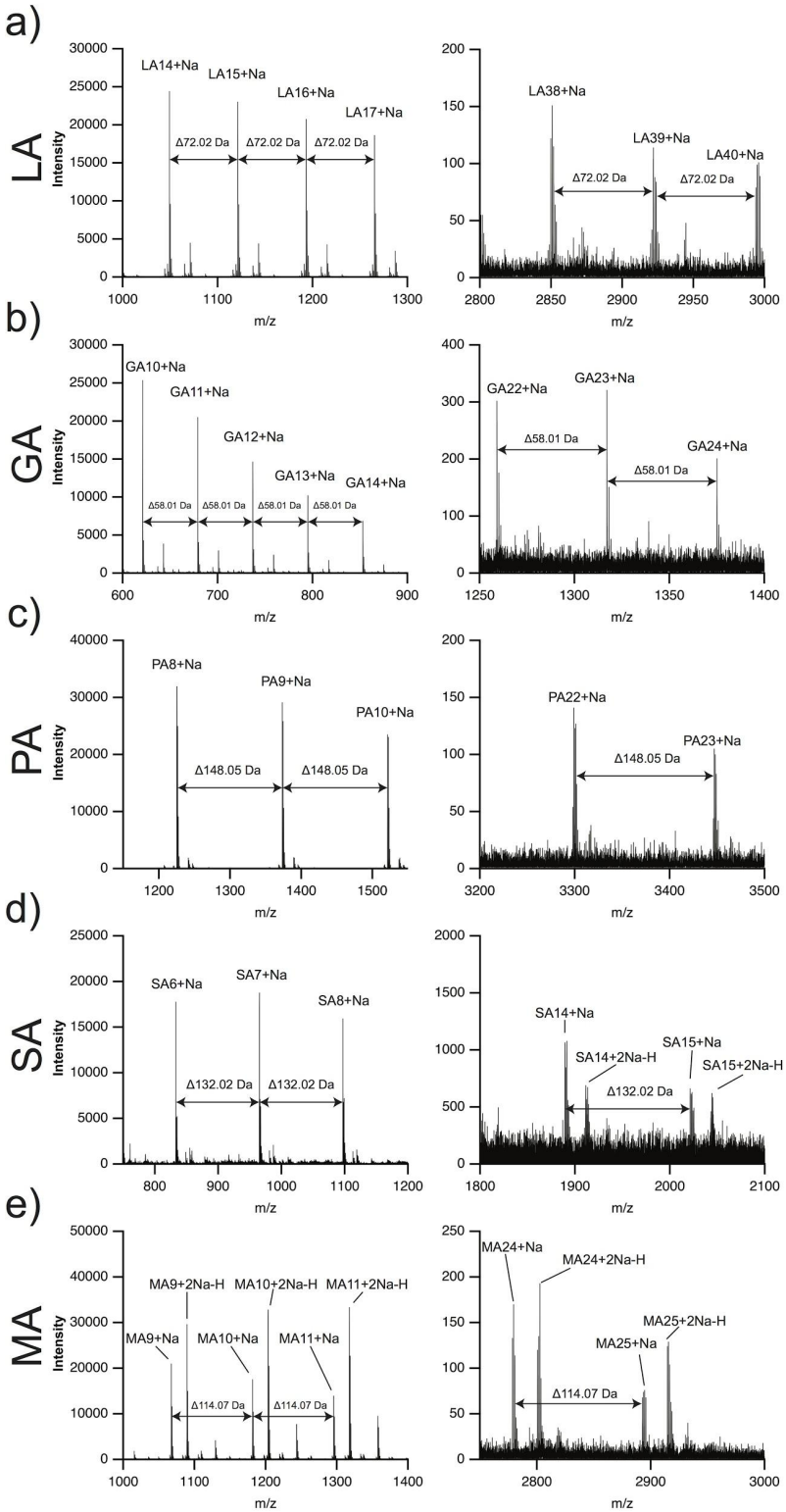

Supplementary Figure S2. Zoomed in MALDI spectra for Fig. S1. Each shows a mid-spectrum region where the mass ladder difference clearly shows polymerization, as well as an end-spectrum region showing peaks representing the largest detectable polymers for each sample. See Supplementary Tables S1–S5 for detailed peak list.

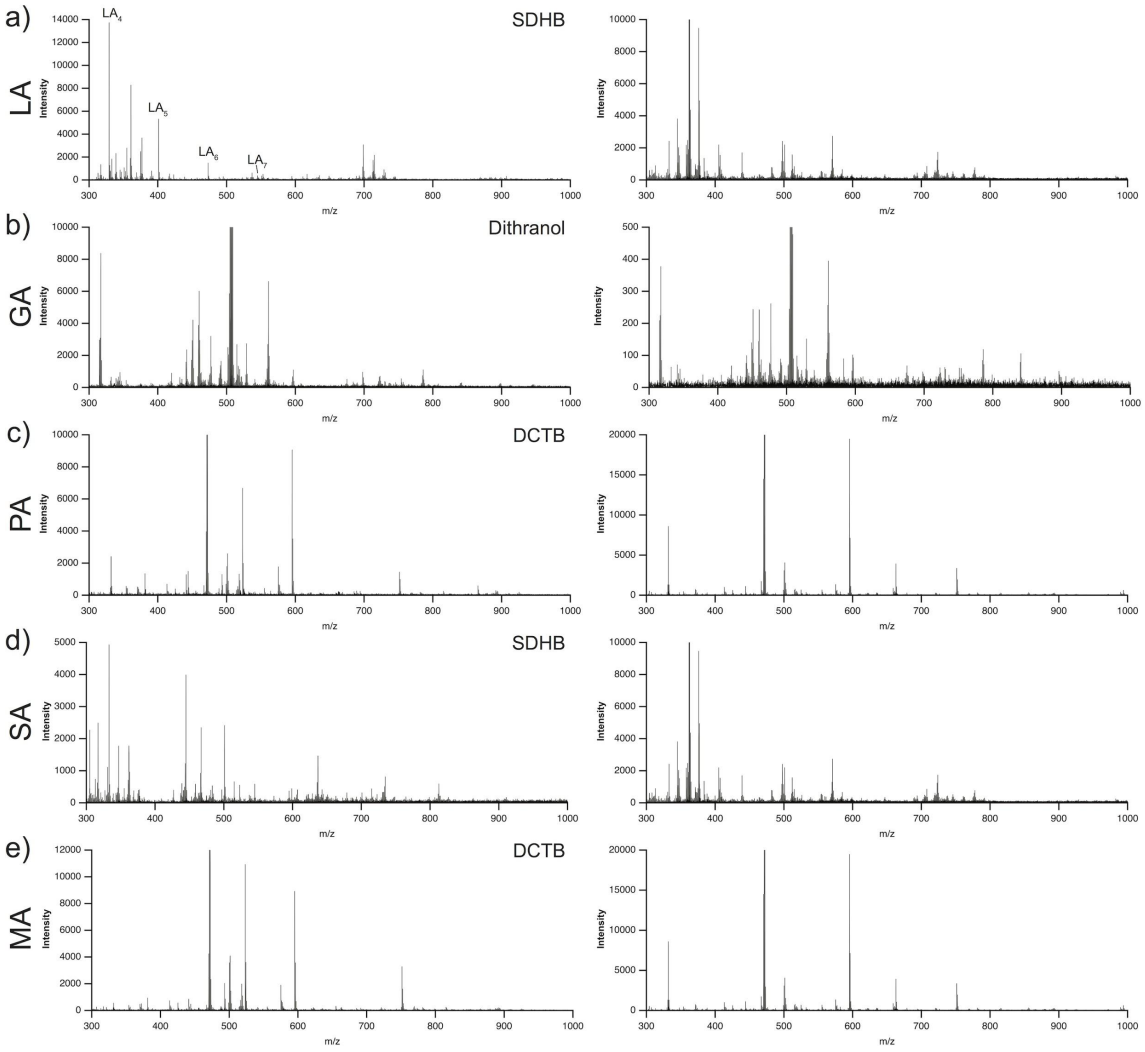

Supplementary Figure S3.
Left: MALDI spectra for unreacted αHA monomers
Right: the accompanying control matrix MALDI spectrum
Except for LA, where small amounts of polymerization up to a 6-mer can be observed, no noticeable polymerization could be detected, suggesting that the condensed phase formed in Fig. S1 is a result of polymerized polyesters of a specific minimum length.

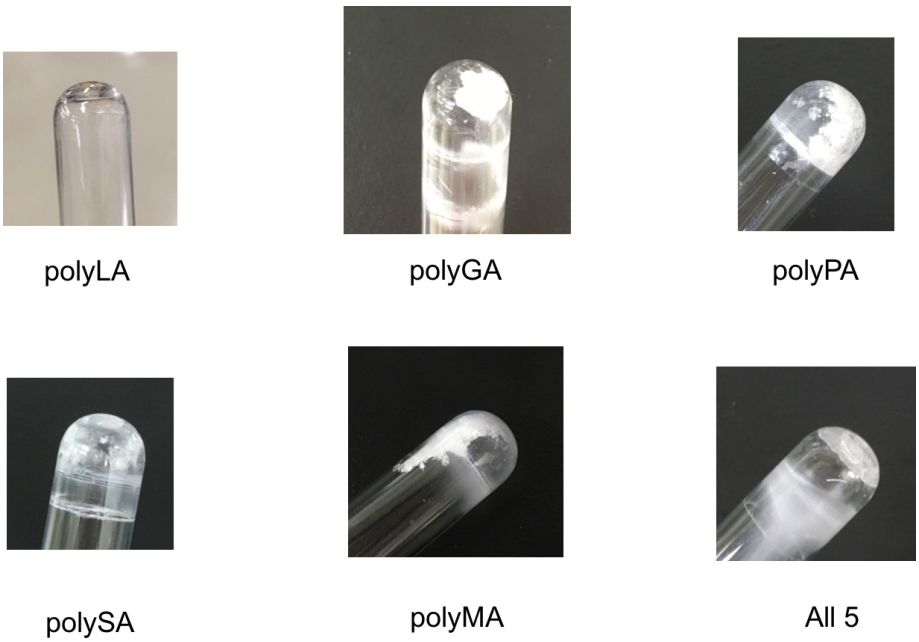

Supplementary Figure S4. Drying of 500 mM of each of the αHAs at 80°C for 2 weeks (same conditions as in Fig. 2), except at pH 7 (using NaOH), did not result in condensed phase formation for any of the samples except polyLA, which still appeared to form a condensed phase after drying.

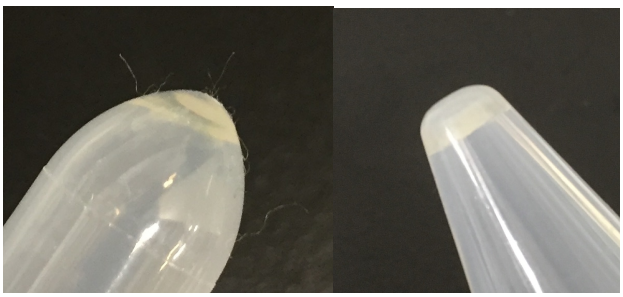

Figure S5. Drying of 500 mM PA at 80°C for 1 week (same conditions as Fig. 2) results in the formation of the same condensed-phase as is observed in the borosilicate glass tubes. The formation of this phase is thus not glass surface-dependent.

Supplementary Figure S6. Sample composed of 100 mM of each of all five αHA (total 500 mM) dried at 80° C for 1 week also formed the gel phases. In fact, all 25 heteropolymer combinations containing two to four different αHAs (i.e., all 10 combinations of two different αHAs, 10 combinations of three different αHAs, and 5 combinations of four different αHAs; photos not shown) formed gel phases.

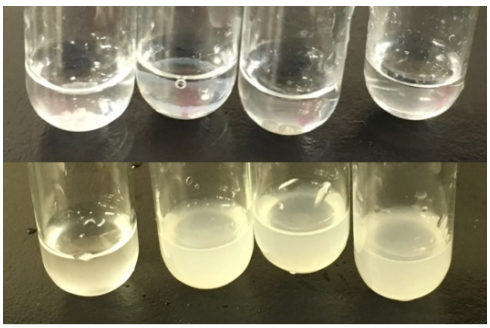

Supplementary Figure S7.
Top: After dissolving in water, sonication, and vortexing, all solutions were still clear, suggesting no (or very little) droplet formation from the condensed phase.
Bottom: However, after addition of 4:1 v/v water:acetonitrile, sonication, and vortexing, all solutions except GA appeared turbid, suggesting droplet formation from the condensed phase.

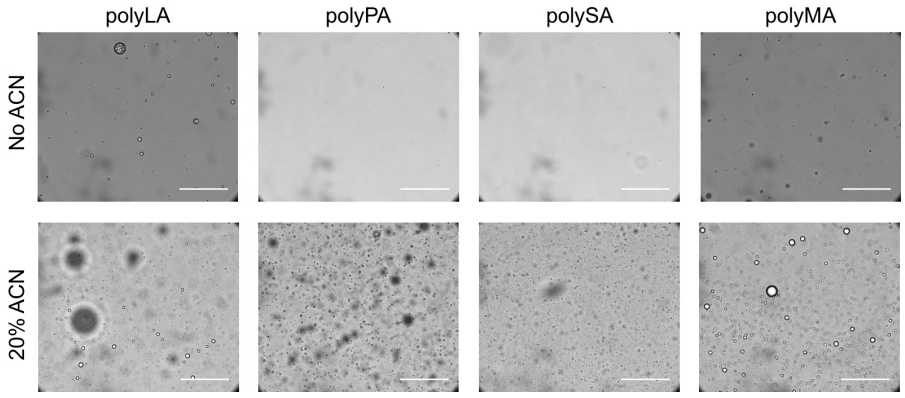

Supplementary Figure S8. Microscopy comparison of various polyester samples upon addition of pure water, or 4:1 v/v water:acetonitrile. In pure water, the droplets were either very few (polyLA and polyMA), or non-existent (polyPA and polySA). However, in 4:1 v/v water:acetonitrile, droplets appeared and were abundant. Thus, we decided to continue with 4:1 v/v water:acetonitrile mixtures for further studies to facilitate formation of smaller microdroplets.

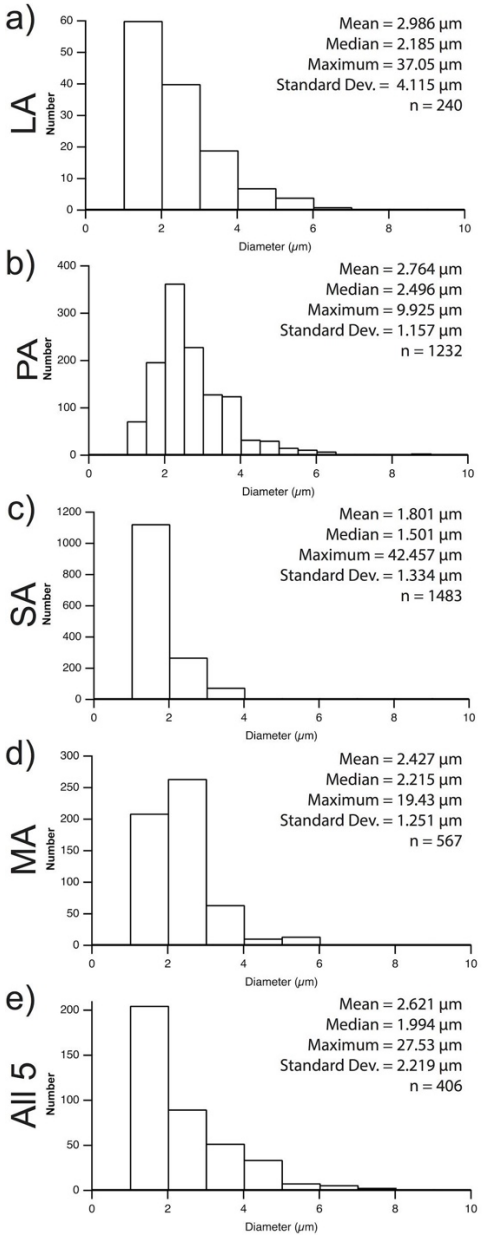

Supplementary Figure S9. Histograms showing size distributions of the spherical particles (diameter in µm) from each image in Fig. 2 (except polyGA). The mean, median, maximum, and standard deviation of particle diameters and the number of particles (**n**) detected are also provided for each image. Image analysis was performed using the microscopy figures in Fig. 2 by FIJI. default thresholding was used, in addition to the "Analyze Particles" function with **Size = (1.05 – infinity)** and **Circularity = 0.00 – 1.00**, while excluding any particles detected that resided on the edge of the image (except in the case of the polyMA sample heated to 90°C, where there was clearly one large particle that would not have been counted properly), particles which were smaller than 10 pixels (Area = 0.104–1.041 μm^2), and large areas which were clearly not particles (which were caused by patches of heterogeneous background intensity typically at the edges of the image that were incorrectly identified as particles). We assumed that all particles were spheres, and back-calculated the diameter of each particle from its computed area.

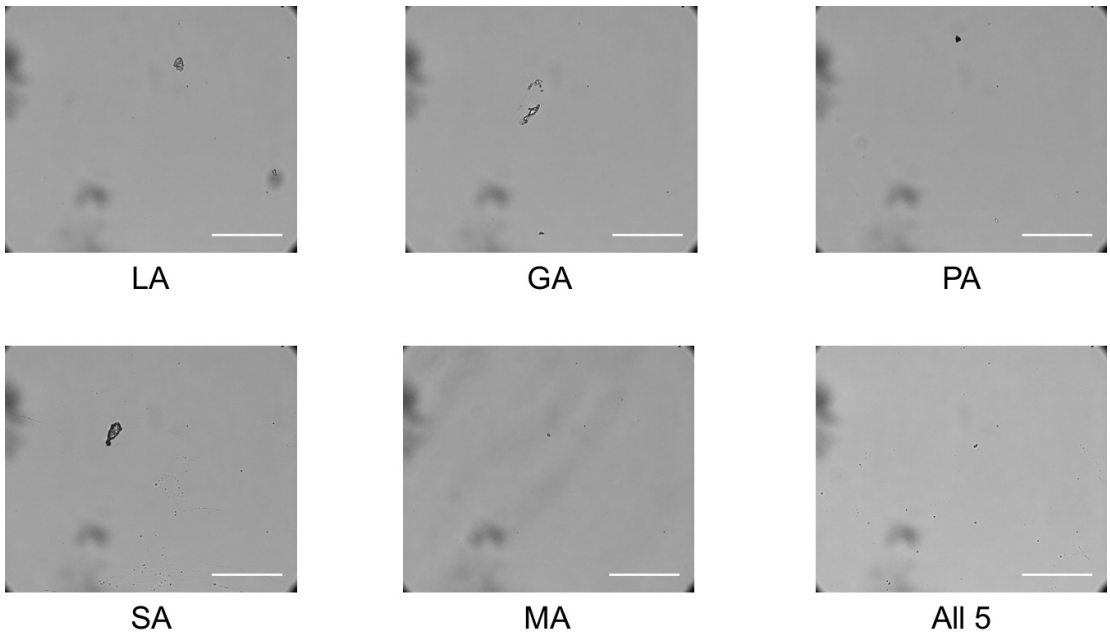

Supplementary Figure S10. Unpolymerized aqueous αHA (500 mM) showed no gel phase or spherical droplets. Scale bars are 100 μm.

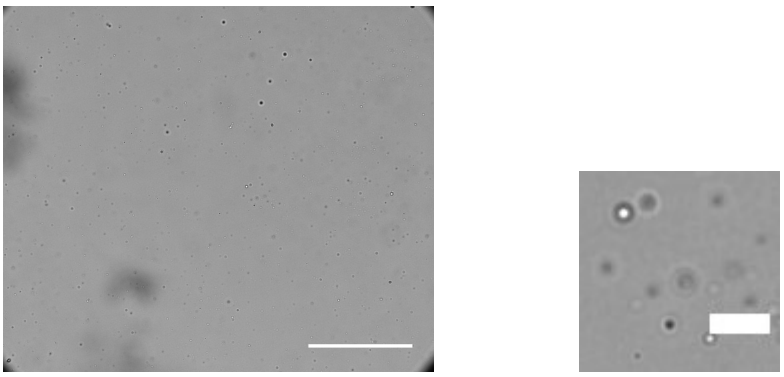

Supplementary Figure S11. Drying at room temperature for 2 months did not result in condensed phase formation except in the case of polyMA (shown: 500 mM MA). Scale bar is 100 μm on the left, 10 μm on the zoom-in on the right.

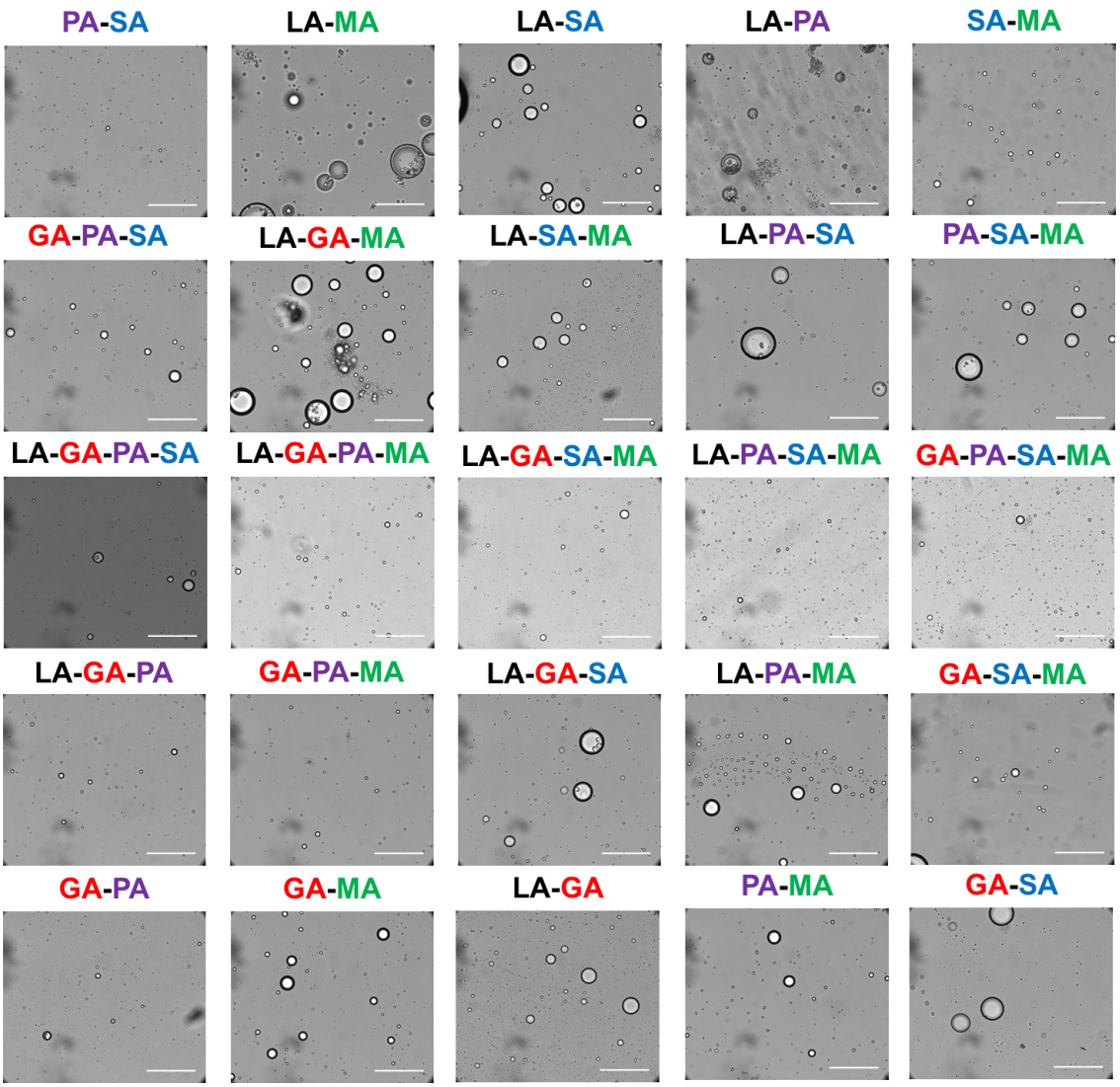

Supplementary Figure S12. Microscope images of all heteropolyester combinations. Each of the combinations formed microdroplets in 4:1 water:acetonitrile. Scale bars are 100 µm. Total concentrations for each reaction (500 µL, 80°C, 1 week) were 500 mM (*e.g.*, in a sample with four αHAs, each αHA would have a concentration of 125 mM).

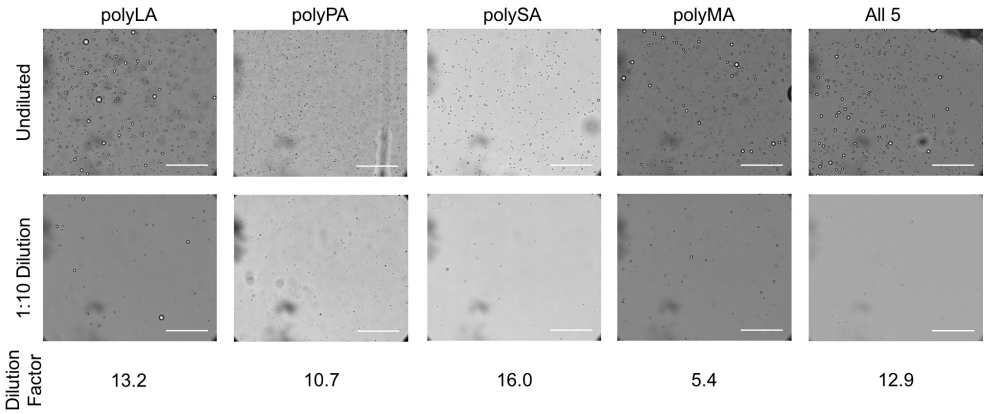

Supplementary Figure S13. Dilution of microdroplets (same conditions as Fig. 2) 1:10 into water does not cause droplet disappearance, as in the case of aqueous two-phase systems (ATPS) and coacervates, whose assembly is concentration-dependent and dilution results in droplet disassembly (1–4). Rather, after 10-fold dilution in water, the number of droplets in the frame is decreased by a factor of ~5.4 – ~16.0, roughly concordant with the dilution factor. Scale bars are 100 μm.

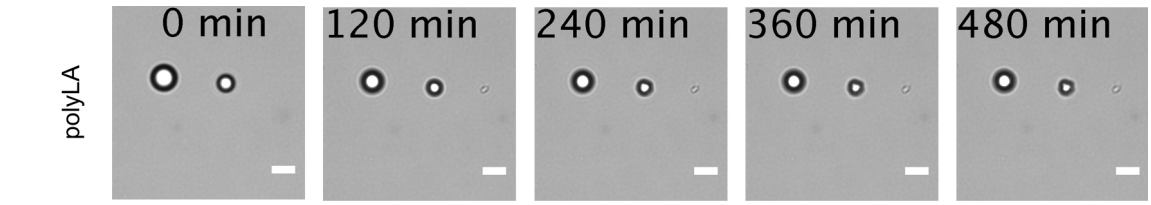

	0 min	120 min	240 min	360 min	480 min
Left Droplet Radius (μm)	9.35	7.58	7.42	6.61	6.62
Right Droplet Radius (μm)	6.29	5.36	4.68	4.68	4.68

Supplementary Figure S14. Dilution of polyLA microdroplets (same conditions as Fig. 2) 1:10 into water (final water:acetonitrile ratio of 49:1 (v/v)) results in a slight decrease in the particle size over many hours in addition to some droplet deformation, potentially caused by slow leaching of lower molecular weight species over time. Particle size was determined by taking an image intensity kymograph in FIJI along a radial axis of the droplet, and measuring the distance between the minima. Scale bars are 10 μm. See Movie S1.

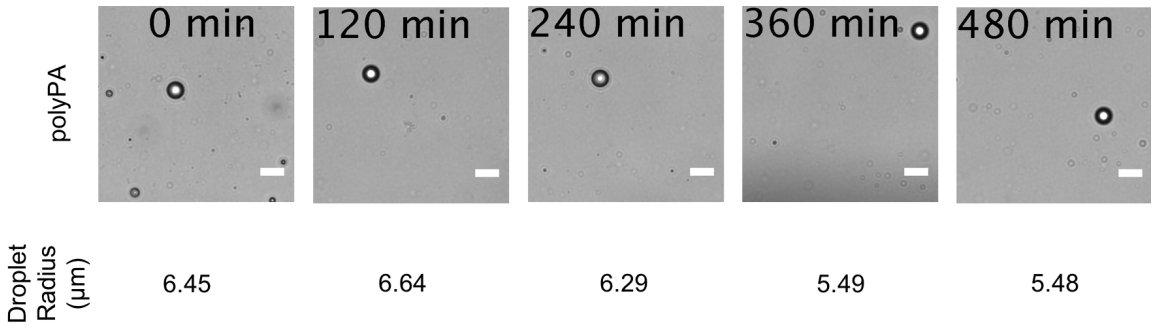

Supplementary Figure S15. Dilution of polyPA microdroplets (same conditions as Fig. 2) 1:10 into water (final water:acetonitrile ratio of 49:1 (v/v)) results in a slight decrease in the particle size over many hours, although apparently to less extent than polyLA microdroplets, potentially suggesting that polyPA droplets are more stable than polyLA droplets. Particle size was determined by taking an image intensity kymograph in FIJI along a radial axis of the droplet, and measuring the distance between the minima. Scale bars are 10 µm. See Movie S2.

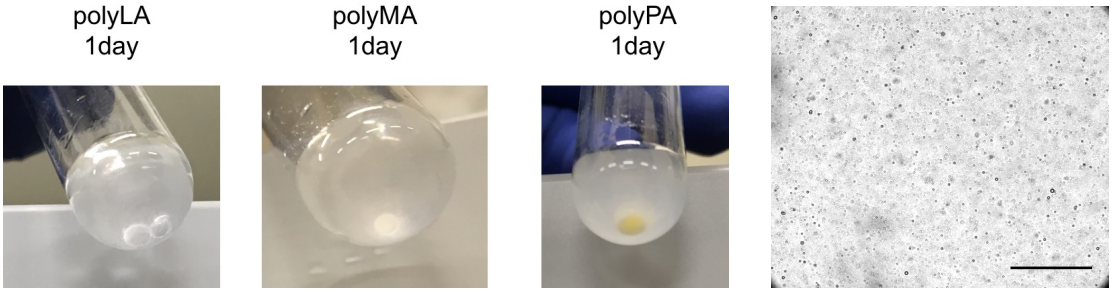

Supplementary Figure S16. After one day of quiescent incubation at room temperature, the droplets begin to coalesce macroscopically (data shown for polyLA, polyMA, polyPA) or oil-like immiscible rafts in aqueous solution (polySA, mixed five αHA sample; not shown); same conditions as Fig. 2. However, the turbidity of the solutions still suggests the presence of droplets or aggregates that have not completely coalesced, which is shown in the microscope image on the right for the polyPA "supernatant" visualized after 2 days. See Movies S3–S4, which show that at short timescales (around one hour), coalescence is generally not observable. Scale bar is 100 μm.

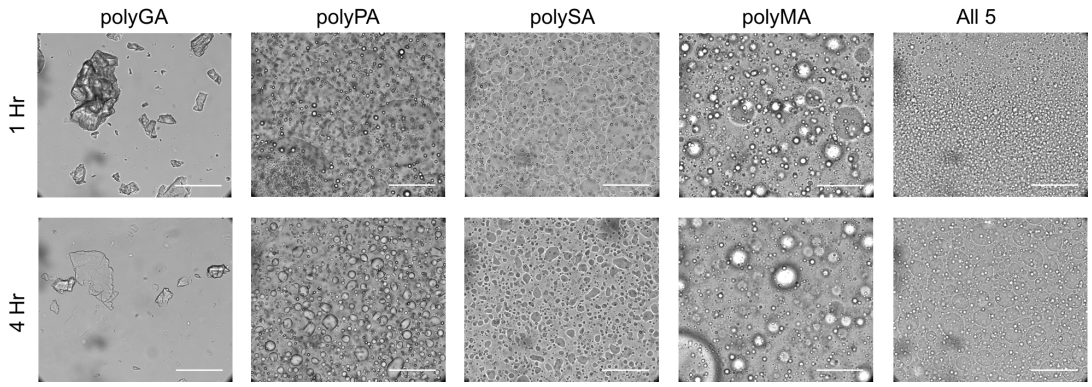

Supplementary Figure S17. Time course showing the variance in pH stability at pH 8 of different polyester microdroplet samples (same conditions as Fig. 2, 800 mM Na-HEPES pH 8). Scale bars are 100 μm. Note: polyGA does not form microdroplets (see Fig. 2).

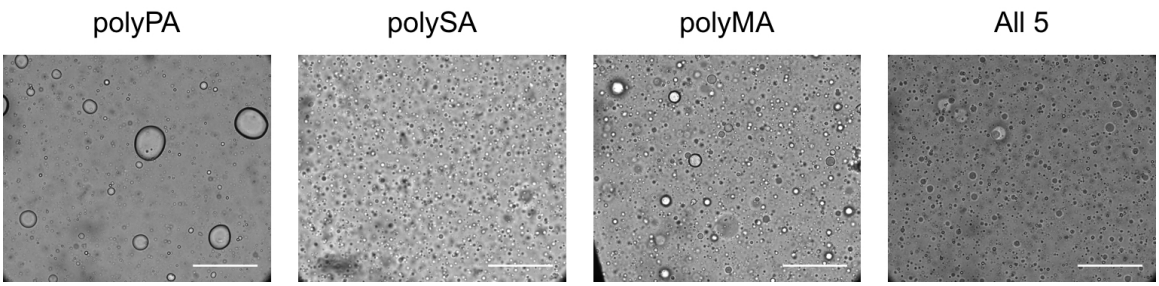

Supplementary Figure S18. Different polyester microdroplet samples after 24 hours of incubation in 800 mM pH 8 Na-HEPES (same conditions as Fig. 2), followed by vortexing. Scale bars are 100 μm.

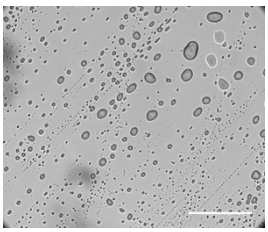

Supplementary Figure S19. After 5 minutes of pH 8 (800 mM Na-HEPES) incubation, polyLA (same conditions as Fig. 2) no longer forms spherical microdroplets. Rather, the microdroplets coalesce rapidly and more easily adhere to the glass coverslip surface, which results in a non-spherical shape. Scale bar is 100 μm.

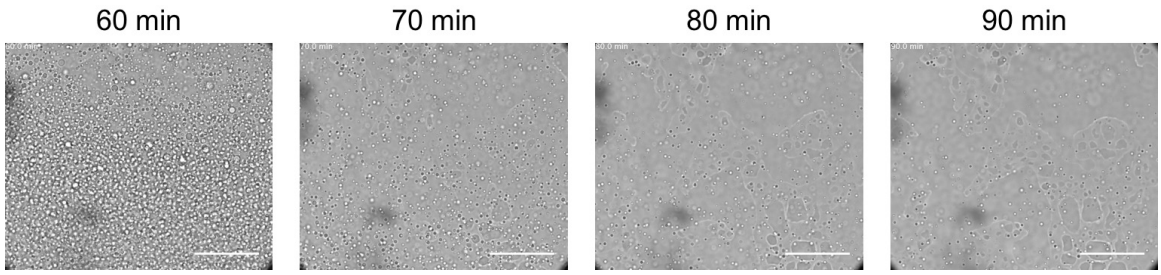

Supplementary Figure S20. At pH 8 (800 mM Na-HEPES), although initially the microdroplets are still able to form (sample containing all five αHAs, same conditions as Fig. 2), they are much less independently stable and coalesce at a much faster rate than when the droplets are present in aqueous solution at pH 2–3, as there are noticeable pools of coalesced structures appearing while the number of total microdroplets decreases (a visibly noticeable thin film was also present in the test tube itself). Sonication after formation of these pools results in reformation of the microdroplets. Supplementary Movie S5 depicts the time between 1 and 1.5 hours after adjusting the pH to 8. Scale bars are 100 μm.

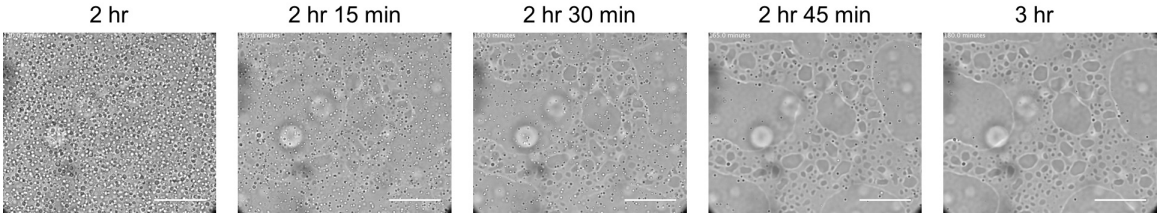

Supplementary Figure S21. Images depict the time between 2 and 3 hours after adjusting a polyPA sample to pH 8 in 800 mM Na-HEPES (same conditions as Fig. 2). Scale bars are 100 μm. See Supplementary Movie S6.

Supplementary Figure S22. Incubation of a vortexed polyPA sample in 100 mM NaCl for 40 minutes (same conditions as Fig. 2) results in the rapid coalescence of the droplets to form a single large macroscopic droplet. This is in contrast to the samples at low pH (2–3), which require about one day to coalesce macroscopically (Fig. S16).

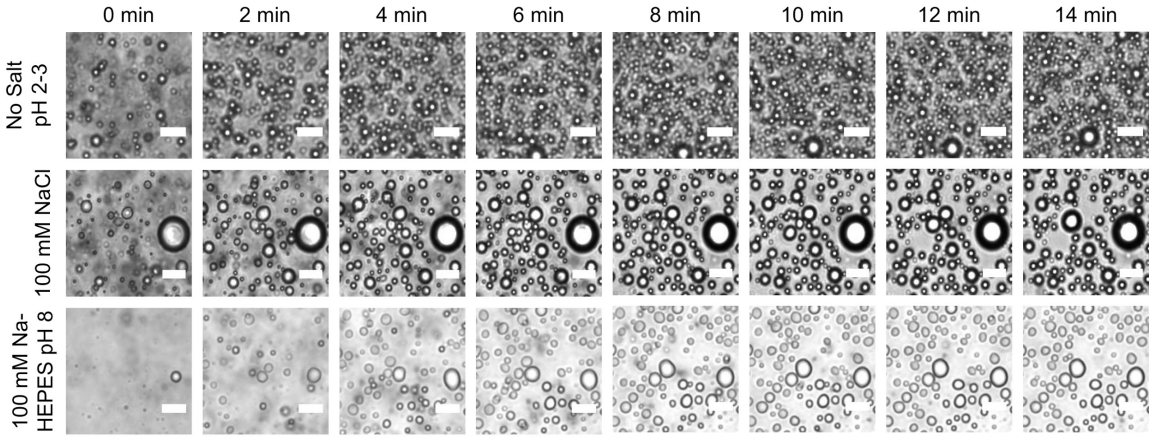

Supplementary Figure S23. Microscopic observation of a polyPA droplets (Same conditions as Fig. 2), in 100 mM NaCl, and 100 mM Na-HEPES, at pH 8. We observe the rapid real-time coalescence of the polyPA droplets in salt and buffered conditions (see Movies S7–S9), while those in standard conditions don't seem to coalesce on this timescale. In contrast, coacervate droplets immediately disassemble upon large pH changes (5), while fatty acid vesicles may avail a larger range of pH-stability upon the incorporation of aliphatic alcohols (6). Scale bars are 10 μm.

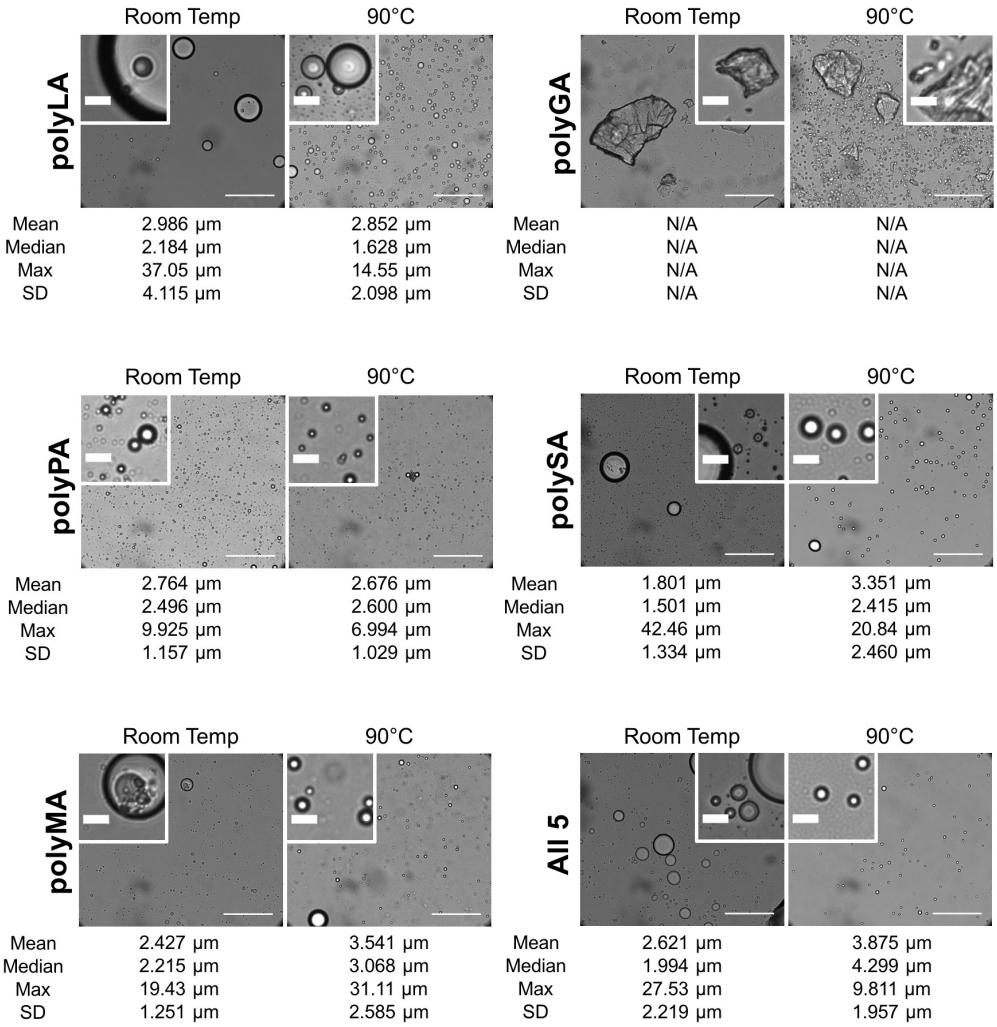

Supplementary Figure S24. All polyester microdroplets appeared stable after heating to 90°C for 5 min, followed by cooling to room temperature (shown, same conditions as Fig. 2). There was little quantifiable change in the microdroplets' general spherical structure (except in the case of polyGA, where the structures appear to start disassembling into smaller parts). Similar to myristoleic acid (MA)/monomyristolein (GMM) vesicles (7), fatty acid/alcohol vesicle systems that are often used as a primitive compartment models, raising the temperature did not destroy the polyester microdroplets. (Although heating MA/GMM vesicles for long periods of time results in instability). This is in contrast to coacervate systems, which disassemble upon temperature decrease (4). Variations in the size and abundance of the polyester droplets are attributed to subtle differences in vortexing and sonication time (see *Methods*) as well as the non-uniform distribution of the droplets within the samples. Scale bars are 100 µm in the main images, 10 µm in the insets. The mean, median, maximum (Max), and standard deviation (SD) of droplet diameters in each image are reported.

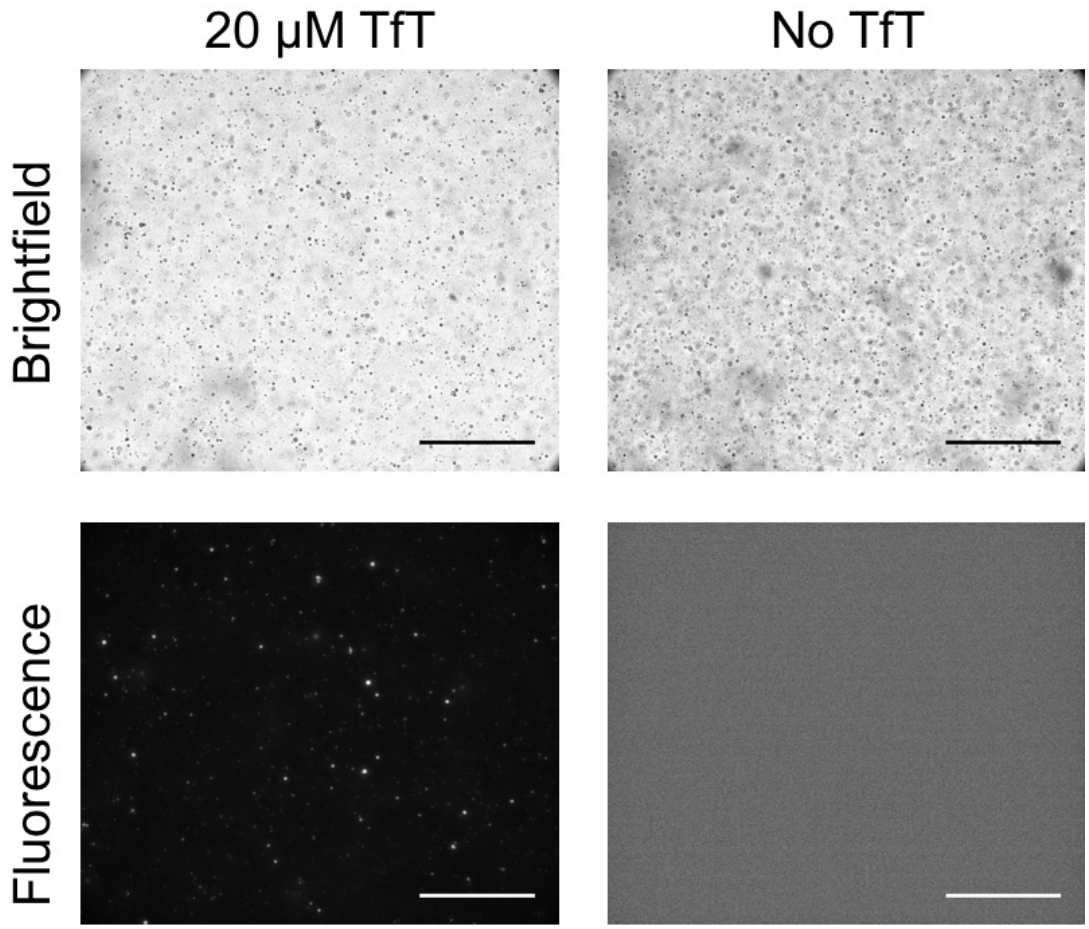

Supplementary Figure S25. PolyPA droplets (created by same conditions as Fig. 2) as visualized by brightfield and fluorescence microscopy (436 nm excitation) with or without 20 μM TfT. The fluorescence images were acquired with the same instrument parameters, which shows that the droplets do not autofluoresce. Scale bar 100 μm.

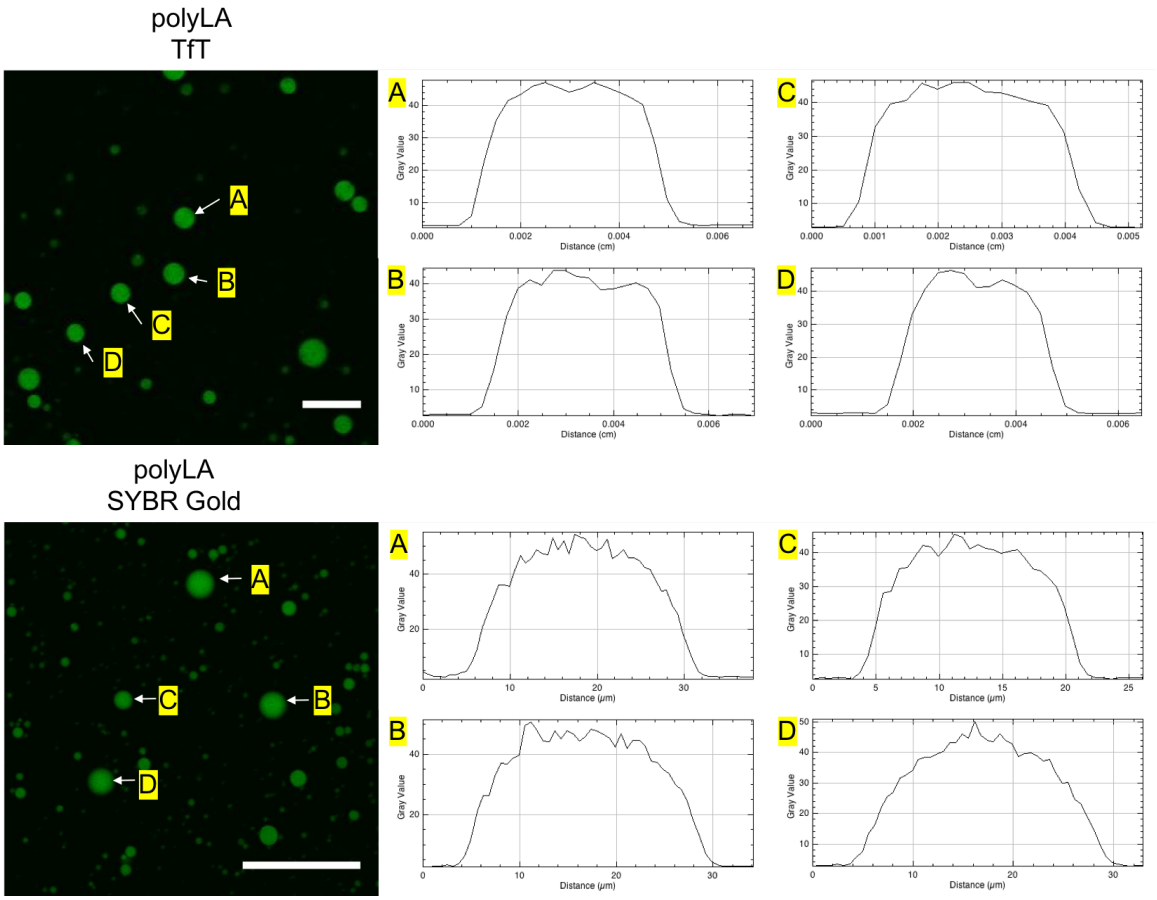

Supplementary Figure S26. Spatial fluorescence intensity analysis of dispersion of TfT and SYBR Gold in polyLA droplets using kymographs generated from the associated confocal microscope image (scale bar 100 μm). The droplets analyzed are indicated as such. Both TfT and SYBR Gold appear to be fairly evenly distributed (due to their non-flat intensity profile (8)) in polyLA droplets, suggesting that the distribution of the polydisperse polyLA products within the droplets may be fairly even).

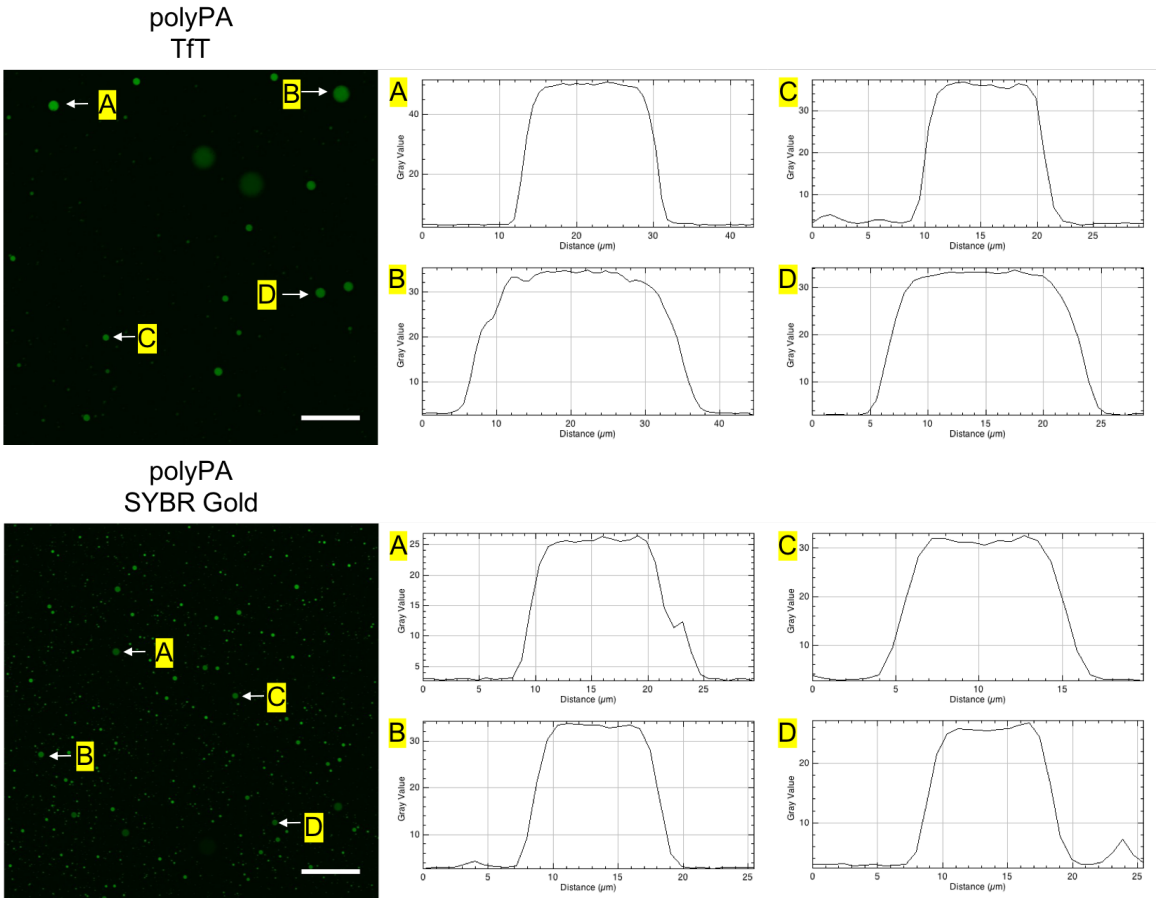

Supplementary Figure S27. Spatial fluorescence intensity analysis of dispersion of TfT and SYBR Gold in polyPA droplets using kymographs generated from the associated confocal microscope image (scale bar 100 μm). The droplets analyzed are indicated as such. Both dyes appear to have a more flat-like intensity distribution, suggesting that perhaps the distribution of the polydisperse polyPA products is not uniform as compared to the polyLA counterparts, possibly due to steric hindrance.

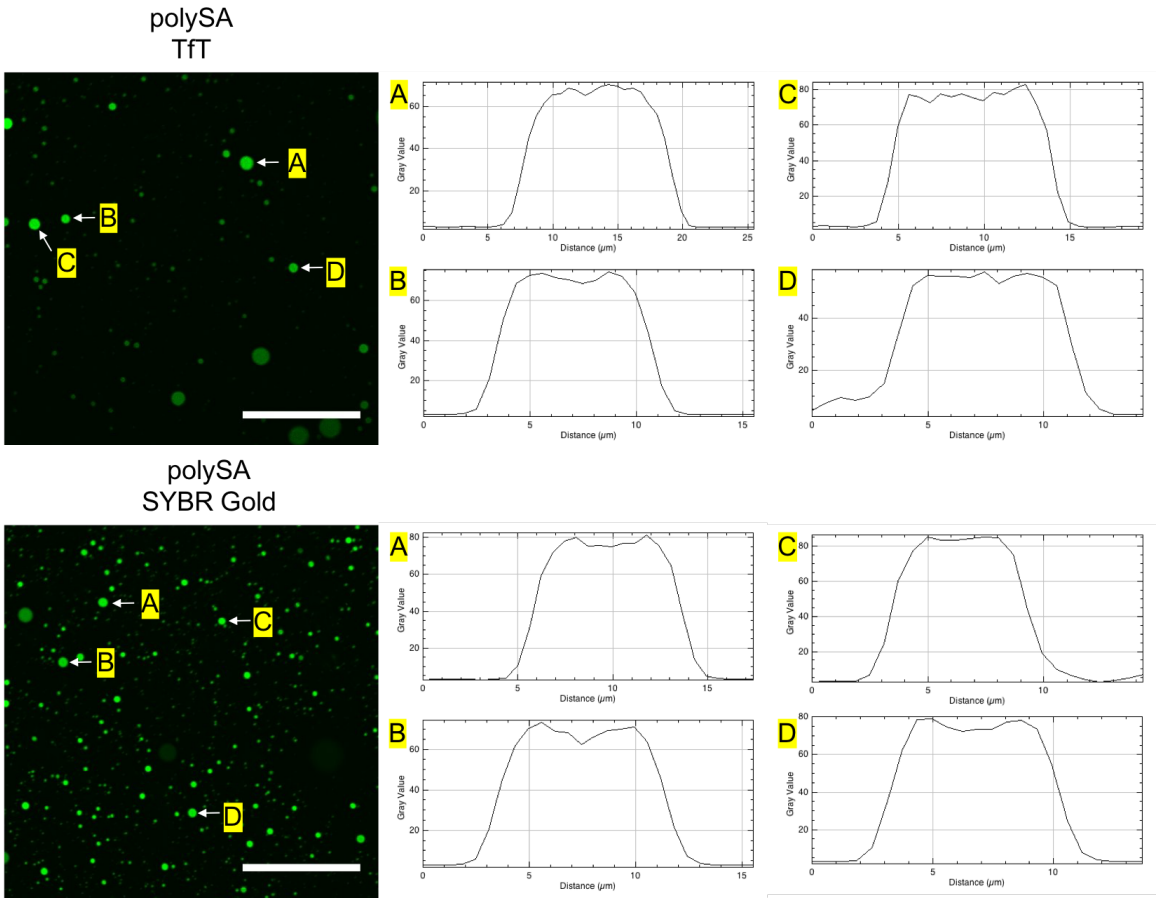

Supplementary Figure S28. Spatial fluorescence intensity analysis of dispersion of TfT and SYBR Gold in polySA droplets using kymographs generated from the associated confocal microscope image (scale bar 100 μm). The droplets analyzed are indicated as such. Both dyes appear to have a more flat-like intensity distribution, and even that the center of the droplets perhaps have lower intensity than the droplet exterior, suggesting that the distribution of the polydisperse polySA products is not uniform as compared to the polyLA counterparts.

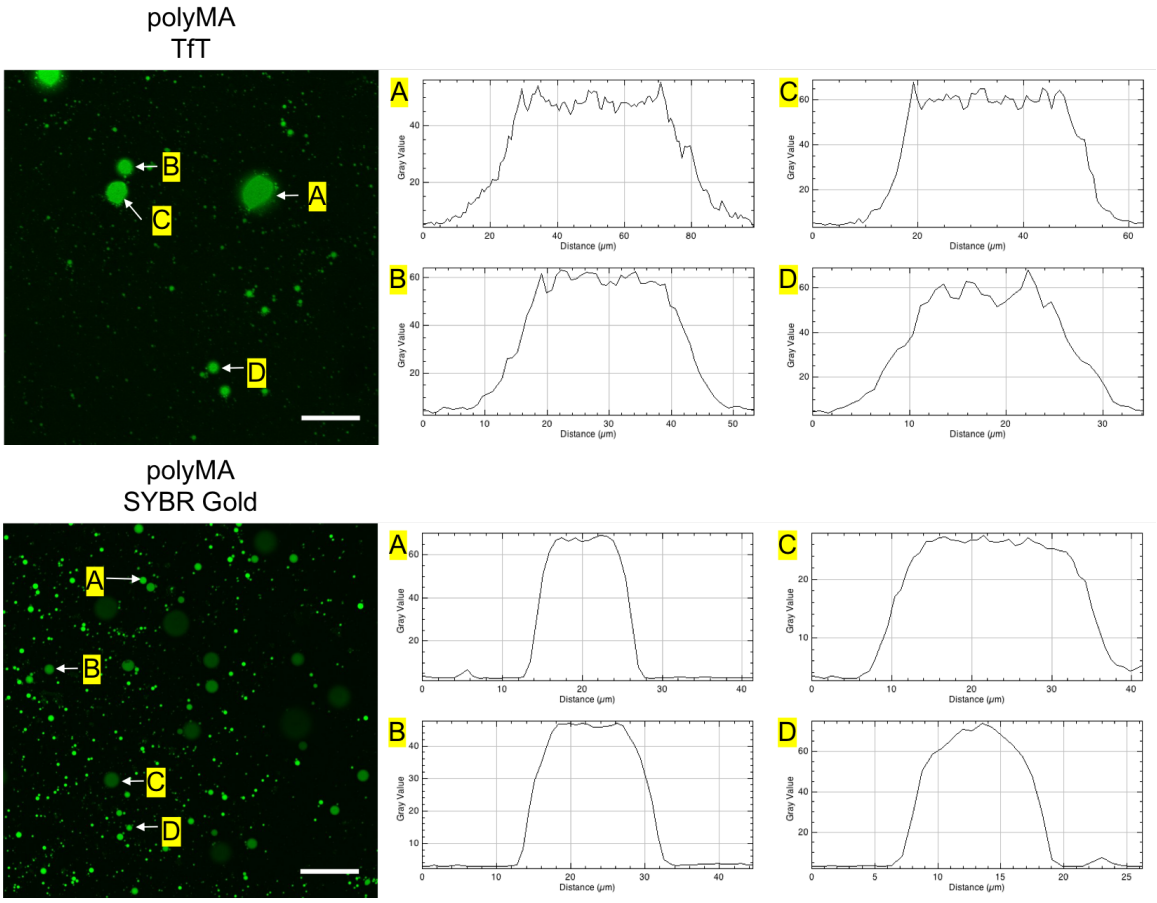

Supplementary Figure S29. Spatial fluorescence intensity analysis of dispersion of TfT and SYBR Gold in polyMA droplets using kymographs generated from the associated confocal microscope image (scale bar 100 μm). The droplets analyzed are indicated as such. For these two dyes, we observe both flat distributions as well as slightly more Gaussian-like distributions, and thus we may not be able to make any strong conclusions about the distribution of the polydisperse polyMA products.

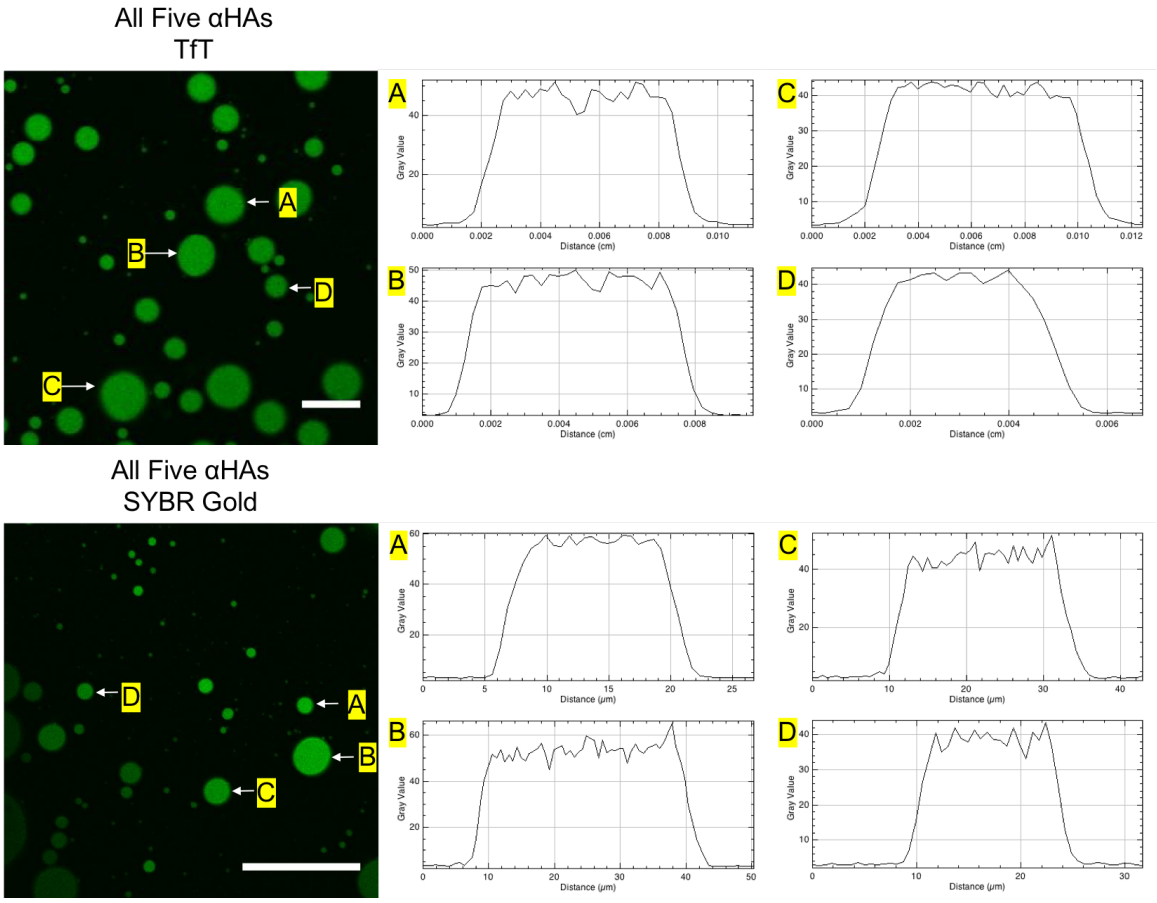

Supplementary Figure S30. Spatial fluorescence intensity analysis of dispersion of TfT and SYBR Gold in droplets generated from synthesizing polyesters from all five αHAs using kymographs generated from the associated confocal microscope image (scale bar 100 μm). The droplets analyzed are indicated as such. Both dyes appear to have a more flat-like intensity distribution, suggesting that perhaps the distribution of the polydisperse products is not uniform.

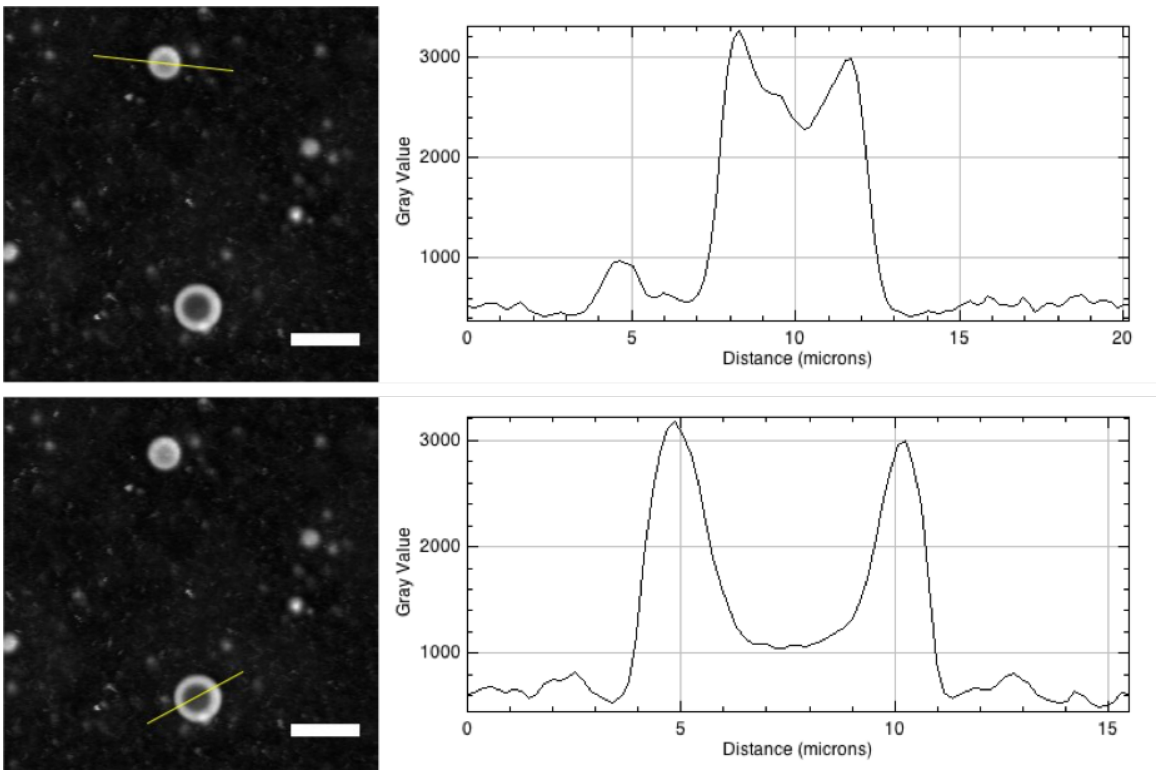

Supplementary Figure S31. Confocal fluorescence microscopy image and radial kymograph of 2 μM Rhodamine-PE (Lissamine™ Rhodamine B 1,2-dihexadecanoyl-*sn*-glycero-3-phosphoethanolamine, triethylammonium salt) in the presence of polyPA droplets (same conditions as Fig. 2) in 200 mM MES pH 5.7. The amphiphilic dye localizes to the exterior of the droplet forming a lipid layer around the droplets (it is unclear these are monolayers), in some cases very strongly, suggesting that the hydrophobic-hydrophilic droplet interface is amenable to assembly of lipid amphiphiles around it. Scale bar is 10 μm.

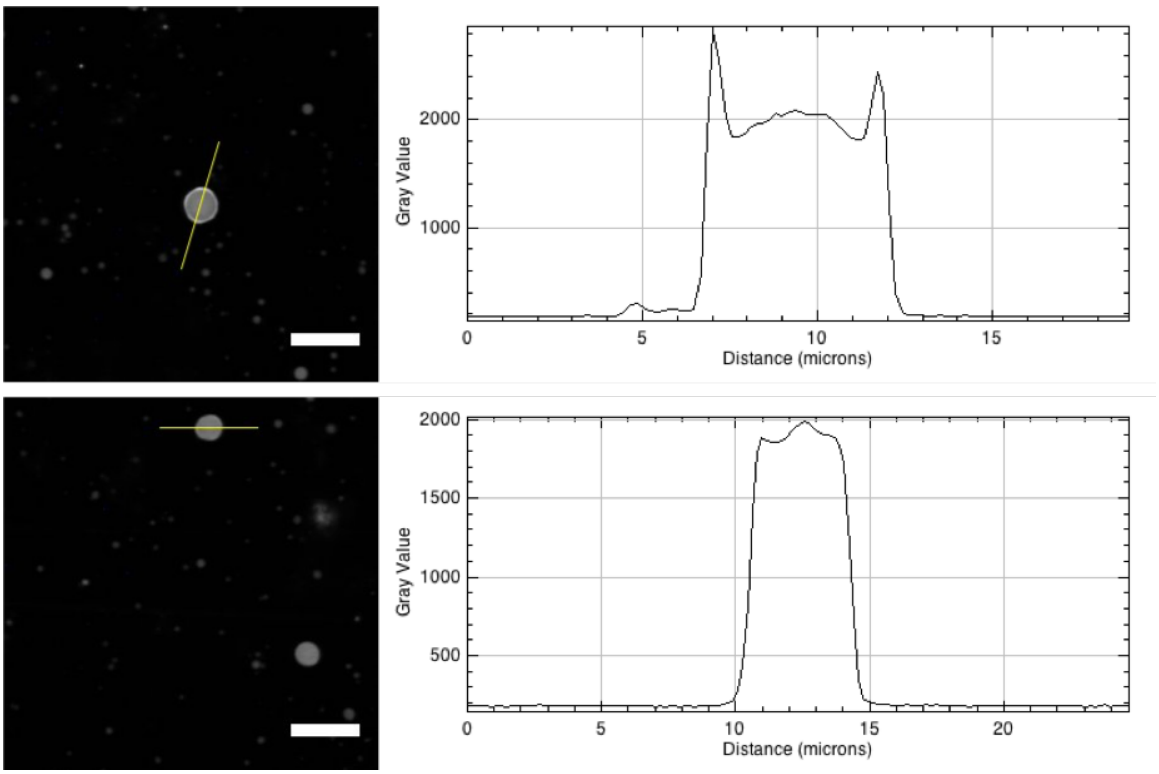

Supplementary Figure S32. Confocal fluorescence microscopy image and radial kymograph of 2 μM Rhodamine-PE in the presence of polySA droplets (same conditions as Fig. 2) in 200 mM MES pH 5.7. We observed droplets which both exhibited increased fluorescence at its exterior (top), as well as those which do not, suggesting that the hydrophobic-hydrophilic interface of polySA may be less pronounced than that of polyPA. Nevertheless, assembly of amphiphilic lipids on some polySA droplets was observed. Scale bar is 10 μm.

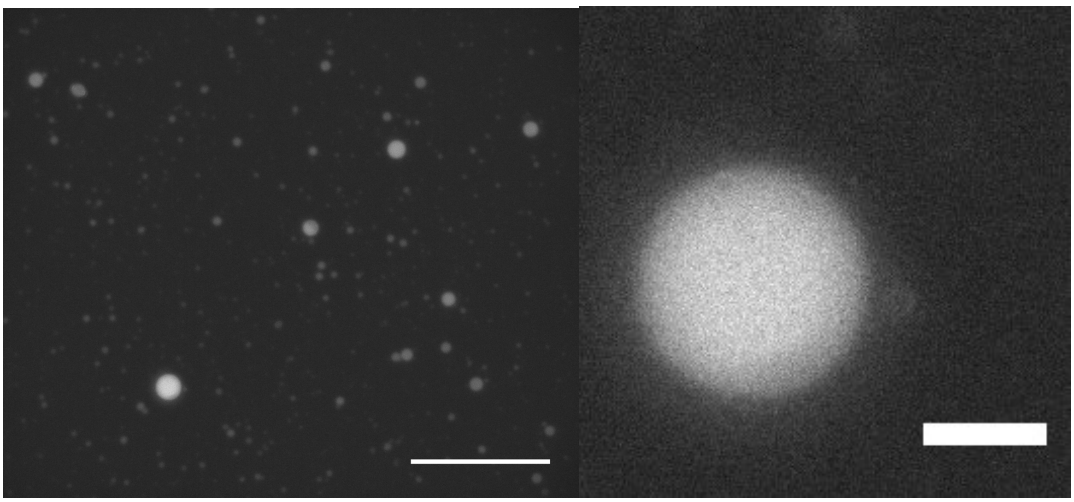

Supplementary Figure S33. Epifluorescence microscope image of polyPA droplets (same conditions as Fig. 2) containing functional *in vitro* expressed and purified superfold green fluorescent protein (sfGFP) (1:80 final dilution; 0.05 mg/mL) in 200 mM MES pH 5.7. This suggests that proteins or peptides could have functioned within such polyester microdroplets, further giving credence to their use as primitive membraneless protocell models. Scale bar on left is 100 μm, scale bar on right is 10 μm.

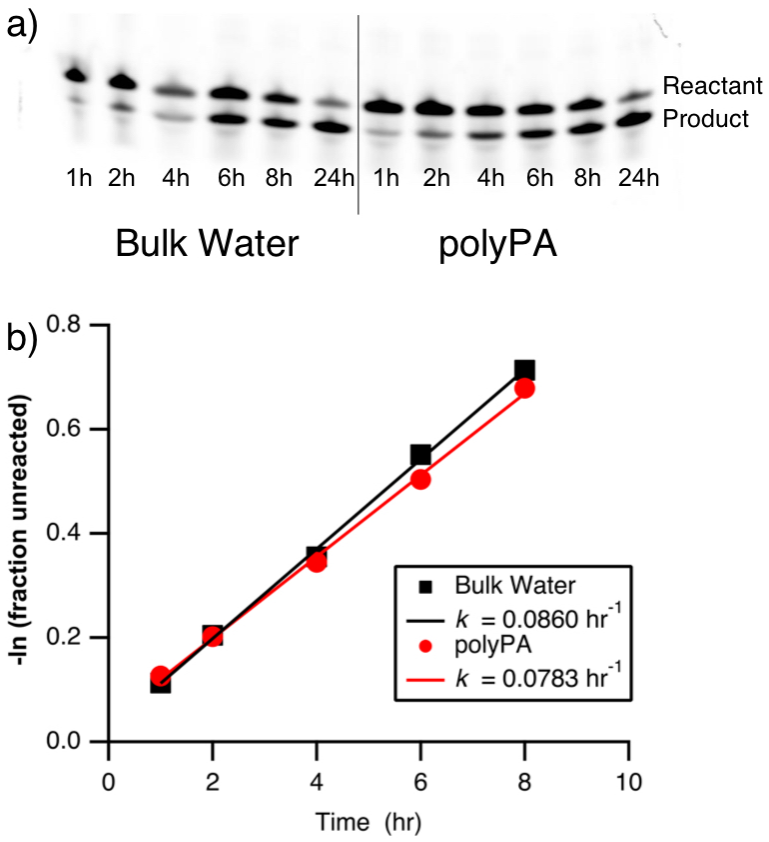

Supplementary Figure S34. Hammerhead Ribozyme Reaction Kinetics in the Presence of polyPA. a) Representative gel-shift assay time course of a hammerhead ribozyme self-cleavage reaction in 100 mM $MgCl_2$, 200 mM MES pH 5.7 in the presence of polyPA (final water:acetonitrile ratio of 85:15 (v/v), *Supplementary Methods*) or in pure water. b) The associated kinetic fit for the reaction including *k*, the first-order rate constant for each reaction. The half life for the reaction in bulk water was 8.05 hours, and the reaction in the presence of polyPA was 8.85 hours.

System	*k*	*k*	*k*	*k*	Average(SEM)
Bulk Water	.1025	0.0860	.0500	.0626	.075(20)
polyPA	.0725	0.0783	.0455	.0423	.060(16)

Supplementary Figure S35. Hammerhead ribozyme cleavage kinetics data summary for all reaction trials in the presence of polyPA or in water. SEM is standard error to the mean. See *Methods* for detailed fitting parameters.

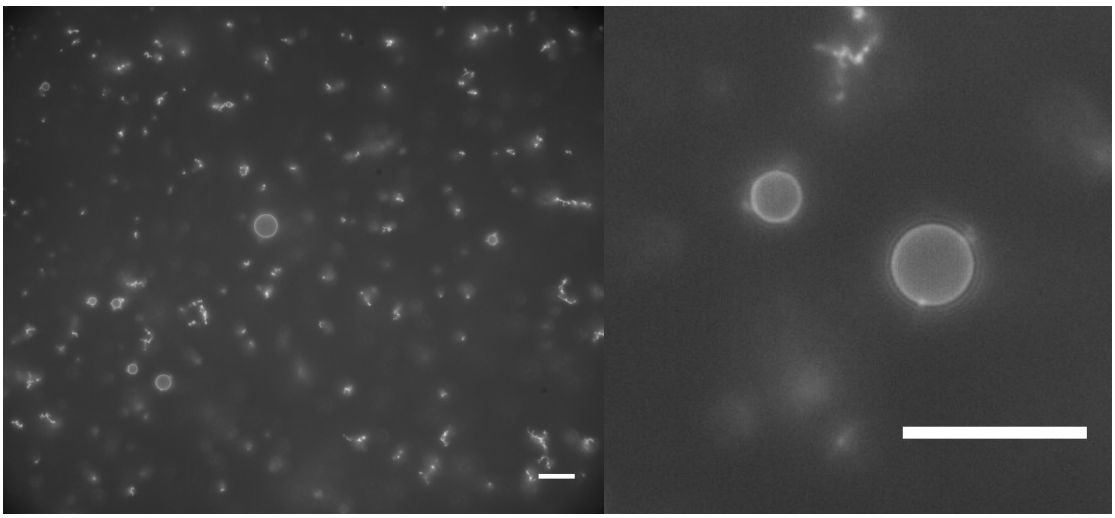

Supplementary Figure S36. Epifluorescence microscope image of polyPA droplets (same conditions as Fig. 2) in the presence of 10 μM fluorescent RNA (5′-FAM-CGCGCCGAAACACCGUGUCUCGAGC-3′), 200 mM MES pH 5.7, and 100 mM $MgCl_2$ after 8 hours of incubation at room temperature. Even after 8 hours, it appears that some fluorescent RNA localizes to the remaining droplets, some of themselves appear to have decreased in number perhaps due to some hydrolysis and disassembly at pH 5.7. This suggests that after 8 hours, some droplets are still viable and could possibly still segregate fluorescent RNA. These images were taken after mixing of the droplets (by vortexing) after 8 hours, perhaps resulting in re-formation of the small droplets if the droplets initially coalesced quickly into a larger droplet or phase (Figs. S21 and S23). However, even if the droplets coalesced quickly, the RNA would still have segregated to the coalesced form (we did not observe how quickly coalescence occured, if at all, in these conditions due to the small volumes used). The RNA may localize to the droplet edge due to binding to buffer or magnesium ions, which have preference of to remain on the droplet exterior as discussed in Figs. S17–S21 (9). Scale bars are 10 μm.

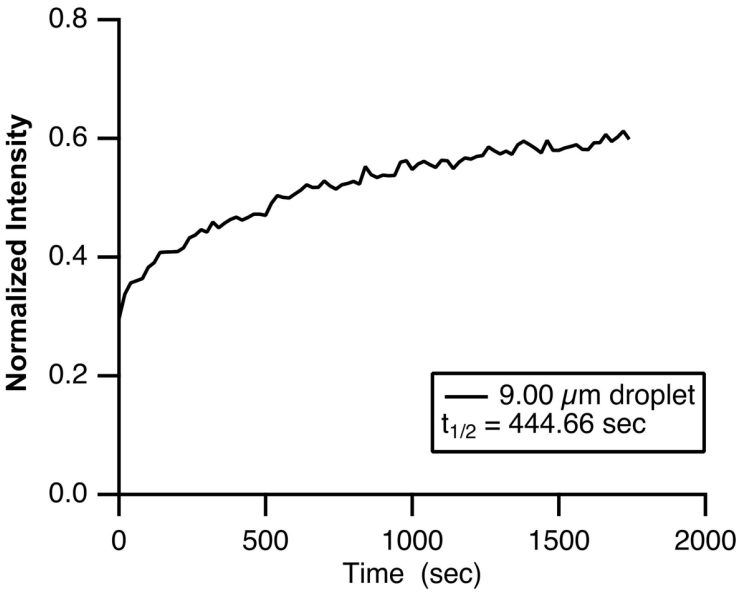

Supplementary Figure S37. Representative fluorescence recovery after photobleaching (FRAP) recovery curve and fitted recovery rate and recovery half time (in duplicate) of 10 μM fluorescent RNA (5′-FAM- CGCGCCGAAACACCGUGUCUCGAGC -3′) in polyPA droplets (same conditions as Fig. 2), with no pH adjustment. The fluorescence recovery half time is on the order of several minutes, suggesting that the RNA is still exchanging with the outside bulk solution to some extent. Although the RNA preferentially segregates within the droplets, we cannot rule out the possibility that the self-cleaving reaction itself occurs when the RNA exchanges out into the bulk solution, before potentially resegregating into the droplet. See Table S6 and Movie S12.

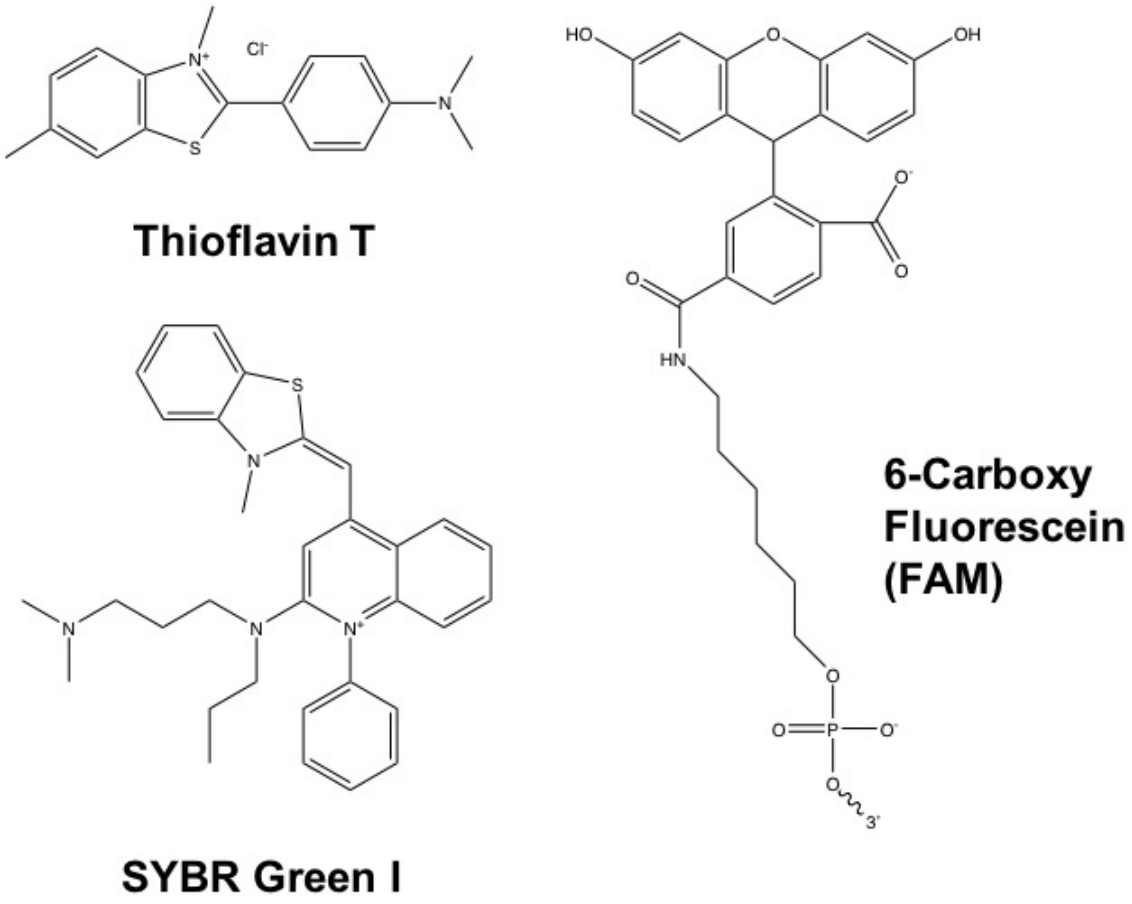

Supplementary Scheme S1. Structures of the dyes in Figure 3. Thioflavin T (TfT) is often used for visualization of amyloids (10), SYBR Gold is used as a chelating dye to visualize nucleic acids (11), and FAM (6-carboxyfluorescein) is a general fluorescent dye often tagged to other biomolecules such as nucleic acids (12). The structure of SYBR Green I is shown rather than SYBR Gold as the structure of SYBR Gold is proprietary and is unavailable publicly; however, SYBR Gold is also an asymmetric cyanine dye, and known to be a modified version of SYBR Green I, and thus the chemical structures should be somewhat similar.

Supplementary Table S1. Peak List for polyLA MALDI (Fig. S1); sodiated peaks.

Observed Mass (Da)	Intensity	Calc. Mass (amu)	Adduct	Polymer	Error (ppm)
329.0917	123	329.0842	M+Na	LA4	22.8
401.1009	492	401.1053	M+Na	LA5	11.1
473.1160	1292	473.1264	M+Na	LA6	22.0
495.1063	200	495.1084	M+2Na-H	LA6	4.2
545.1430	4013	545.1475	M+Na	LA7	8.3
567.1176	443	567.1295	M+2Na-H	LA7	20.9
617.1567	8562	617.1687	M+Na	LA8	19.3
639.1333	1040	639.1506	M+2Na-H	LA8	27.1
689.1732	13437	689.1898	M+Na	LA9	24.0
711.1555	1948	711.1717	M+2Na-H	LA9	22.8
761.1872	18246	761.2109	M+Na	LA10	31.1
783.1741	2942	783.1928	M+2Na-H	LA10	23.9
833.2131	21694	833.2320	M+Na	LA11	22.7
855.1938	4015	855.2139	M+2Na-H	LA11	23.5
905.2280	23735	905.2531	M+Na	LA12	27.8
927.2143	4406	927.2350	M+2Na-H	LA12	22.4
977.2538	24563	977.2742	M+Na	LA13	20.9
999.2353	4700	999.2562	M+2Na-H	LA13	20.9

1049.2755	**24420**	**1049.2953**	**M+Na**	**LA14**	**18.9**
1071.2598	**4490**	**1071.2773**	**M+2Na-H**	**LA14**	**16.3**
1121.3008	**23025**	**1121.3164**	**M+Na**	**LA15**	**14.0**
1143.2859	**4410**	**1143.2984**	**M+2Na-H**	**LA15**	**10.9**
1193.3330	**20759**	**1193.3375**	**M+Na**	**LA16**	**3.8**
1215.3113	**4273**	**1215.3195**	**M+2Na-H**	**LA16**	**6.7**
1265.3601	**18636**	**1265.3586**	**M+Na**	**LA17**	**1.2**
1287.3428	**3443**	**1287.3406**	**M+2Na-H**	**LA17**	**1.7**
1337.3820	**16256**	**1337.3798**	**M+Na**	**LA18**	**1.6**
1359.3710	**3237**	**1359.3617**	**M+2Na-H**	**LA18**	**6.8**
1409.4154	**14008**	**1409.4009**	**M+Na**	**LA19**	**10.3**
1431.4009	**2649**	**1431.3828**	**M+2Na-H**	**LA19**	**12.6**
1481.4431	**12221**	**1481.4220**	**M+Na**	**LA20**	**14.3**
1503.4301	**2494**	**1503.4039**	**M+2Na-H**	**LA20**	**17.4**
1553.4748	**10340**	**1553.4431**	**M+Na**	**LA21**	**20.4**
1575.4540	**2129**	**1575.4250**	**M+2Na-H**	**LA21**	**18.4**
1625.5070	**8657**	**1625.4642**	**M+Na**	**LA22**	**26.3**
1647.4730	**1612**	**1647.4461**	**M+2Na-H**	**LA22**	**16.3**
1697.5289	**6743**	**1697.4853**	**M+Na**	**LA23**	**25.7**
1719.5221	**1247**	**1719.4673**	**M+2Na-H**	**LA23**	**31.9**

1769.5525	**5752**	**1769.5064**	**M+Na**	**LA24**	**26.0**
1791.5330	**1190**	**1791.4884**	**M+2Na-H**	**LA24**	**24.9**
1841.5792	**4403**	**1841.5275**	**M+Na**	**LA25**	**28.0**
1863.5626	**905**	**1863.5095**	**M+2Na-H**	**LA25**	**28.5**
1913.6202	**3092**	**1913.5486**	**M+Na**	**LA26**	**37.4**
1935.5812	**715**	**1935.5306**	**M+2Na-H**	**LA26**	**26.1**
1985.6397	**2579**	**1985.5697**	**M+Na**	**LA27**	**35.2**
2007.6105	**537**	**2007.5517**	**M+2Na-H**	**LA27**	**29.3**
2057.6523	**1956**	**2057.5909**	**M+Na**	**LA28**	**29.9**
2079.6345	**567**	**2079.5728**	**M+2Na-H**	**LA28**	**29.7**
2129.6809	**1548**	**2129.6120**	**M+Na**	**LA29**	**32.4**
2151.6780	**385**	**2151.5939**	**M+2Na-H**	**LA29**	**39.1**
2201.7202	**1251**	**2201.6331**	**M+Na**	**LA30**	**39.6**
2223.6897	**298**	**2223.6150**	**M+2Na-H**	**LA30**	**33.6**
2273.7332	**977**	**2273.6542**	**M+Na**	**LA31**	**34.7**
2295.7173	**188**	**2295.6361**	**M+2Na-H**	**LA31**	**35.4**
2345.7476	**773**	**2345.6753**	**M+Na**	**LA32**	**30.8**
2367.7297	**184**	**2367.6572**	**M+2Na-H**	**LA32**	**30.6**
2417.7715	**575**	**2417.6964**	**M+Na**	**LA33**	**31.1**
2439.7488	**143**	**2439.6784**	**M+2Na-H**	**LA33**	**28.9**

2489.7932	**443**	**2489.7175**	**M+Na**	**LA34**	**30.4**
2511.7629	**182**	**2511.6995**	**M+2Na-H**	**LA34**	**25.3**
2561.8032	**292**	**2561.7386**	**M+Na**	**LA35**	**25.2**
2583.7903	**102**	**2583.7206**	**M+2Na-H**	**LA35**	**27.0**
2633.8211	**308**	**2633.7597**	**M+Na**	**LA36**	**23.3**
2705.8579	**254**	**2705.7808**	**M+Na**	**LA37**	**28.5**
2777.8335	**160**	**2777.8020**	**M+Na**	**LA38**	**11.4**
2849.8569	**122**	**2849.8231**	**M+Na**	**LA39**	**11.9**
2921.8799	**114**	**2921.8442**	**M+Na**	**LA40**	**12.2**

Supplementary Table S2. Peak List for polyGA MALDI (Fig. S1); sodiated peaks.

Observed Mass (Da)	Intensity	Calc. Mass (amu)	Adduct	Polymer	Error (ppm)
215.0305	246	215.0162	M+Na	GA3	66.3
273.0372	359	273.0217	M+Na	GA4	56.9
295.0141	256	295.0036	M+2Na-H	GA4	35.6
331.0386	513	331.0272	M+Na	GA5	34.5
353.0299	287	353.0091	M+2Na-H	GA5	59.0
389.0403	2393	389.0327	M+Na	GA6	19.5
411.0254	733	411.0146	M+2Na-H	GA6	26.3
447.0440	8508	447.0381	M+Na	GA7	13.2
469.0190	1863	469.0201	M+2Na-H	GA7	2.2
505.0437	25888	505.0436	M+Na	GA8	80.2
527.0226	3854	527.0256	M+2Na-H	GA8	5.6
563.0460	26881	563.0491	M+Na	GA9	5.5
585.0319	3922	585.0310	M+2Na-H	GA9	1.4
621.0524	25367	621.0546	M+Na	GA10	3.6
643.0269	3858	643.0365	M+2Na-H	GA10	14.9
679.0536	20502	679.0601	M+Na	GA11	9.5
701.0362	2960	701.0420	M+2Na-H	GA11	8.3
737.0551	14643	737.0655	M+Na	GA12	14.1

759.0352	**2409**	**759.0475**	**M+2Na-H**	**GA12**	**16.2**
795.0594	**10219**	**795.0710**	**M+Na**	**GA13**	**14.6**
817.0413	**1699**	**817.0530**	**M+2Na-H**	**GA13**	**14.2**
853.0683	**6875**	**853.0765**	**M+Na**	**GA14**	**9.6**
875.0452	**1128**	**875.0584**	**M+2Na-H**	**GA14**	**15.1**
911.0758	**3936**	**911.0820**	**M+Na**	**GA15**	**6.8**
933.0552	**805**	**933.0639**	**M+2Na-H**	**GA15**	**9.4**
969.0809	**2715**	**969.0875**	**M+Na**	**GA16**	**6.8**
991.0586	**521**	**991.0694**	**M+2Na-H**	**GA16**	**10.9**
1027.0878	**1598**	**1027.0929**	**M+Na**	**GA17**	**5.0**
1049.0613	**358**	**1049.0749**	**M+2Na-H**	**GA17**	**13.0**
1085.0931	**1029**	**1085.0984**	**M+Na**	**GA18**	**4.9**
1107.0763	**227**	**1107.0804**	**M+2Na-H**	**GA18**	**3.7**
1143.1052	**766**	**1143.1039**	**M+Na**	**GA19**	**1.2**
1165.0856	**162**	**1165.0858**	**M+2Na-H**	**GA19**	**0.2**
1201.1071	**451**	**1201.1093**	**M+Na**	**GA20**	**1.9**
1223.1122	**154**	**1223.0913**	**M+2Na-H**	**GA20**	**17.0**
1259.1220	**302**	**1259.1149**	**M+Na**	**GA21**	**5.6**
1281.1051	**83**	**1281.0968**	**M+2Na-H**	**GA21**	**6.5**
1317.1332	**321**	**1317.1203**	**M+Na**	**GA22**	**9.8**

1339.1043	**91**	**1339.1023**	**M+2Na-H**	**GA22**	**1.5**
1375.1336	**201**	**1375.1258**	**M+Na**	**GA23**	**5.6**
1433.1443	**101**	**1433.1313**	**M+Na**	**GA24**	**9.1**

Supplementary Table S3. Peak List for polyPA MALDI (Fig. S1); sodiated peaks.

Observed Mass (Da)	Intensity	Calc. Mass (amu)	Adduct	Polymer	Error (ppm)
337.1283	146	337.1046	M+Na	PA2	70.1
485.1614	1835	485.1571	M+Na	PA3	9.3
633.2096	6436	633.2095	M+Na	PA4	0.2
781.2611	15964	781.2619	M+Na	PA5	1.0
929.3143	25569	929.3144	M+Na	PA6	0.1
1077.3720	30747	1077.3668	M+Na	PA7	4.8
1225.4360	31932	1225.4192	M+Na	PA8	13.7
1373.5107	29142	1373.4716	M+Na	PA9	28.5
1521.5855	23483	1521.5241	M+Na	PA10	40.3
1669.6493	17530	1669.5765	M+Na	PA11	43.6
1817.7178	12026	1817.6289	M+Na	PA12	48.9
1965.7877	7590	1965.6814	M+Na	PA13	54.1
2113.8572	4754	2113.7338	M+Na	PA14	58.4
2261.9087	2862	2261.7862	M+Na	PA15	54.1
2409.9761	1656	2409.8387	M+Na	PA16	57.0
2558.0147	1164	2557.8911	M+Na	PA17	48.3
2706.0566	547	2705.9435	M+Na	PA18	41.8
2854.1143	329	2853.9959	M+Na	PA19	41.5

3002.1382	**123**	**3002.0484**	**M+Na**	**PA20**	**29.9**
3150.1436	**101**	**3150.1008**	**M+Na**	**PA21**	**13.6**
3298.1245	**54**	**3298.1532**	**M+Na**	**PA22**	**8.7**
3446.1196	**44**	**3446.2057**	**M+Na**	**PA23**	**25.0**

Supplementary Table S4. Peak List for polySA MALDI (Fig. S1); sodiated peaks.

Observed Mass (Da)	Intensity	Calc. Mass (amu)	Adduct	Polymer	Error (ppm)
305.0459	584	305.0488	M+Na	SA2	9.5
327.0266	547	327.0307	M+2Na-H	SA2	12.8
437.0935	2515	437.0733	M+Na	SA3	46.2
459.0807	453	459.0553	M+2Na-H	SA3	55.3
569.0923	5522	569.0978	M+Na	SA4	9.7
591.0963	656	591.0798	M+2Na-H	SA4	27.9
701.1102	12498	701.1223	M+Na	SA5	17.3
723.0966	1230	723.1043	M+2Na-H	SA5	10.6
833.1323	17784	833.1468	M+Na	SA6	17.4
855.1121	1771	855.1288	M+2Na-H	SA6	19.6
965.1575	18773	965.1713	M+Na	SA7	14.4
987.1387	2076	987.1533	M+2Na-H	SA7	14.8
1097.186	15947	1097.1959	M+Na	SA8	8.9
1119.1635	1578	1119.1778	M+2Na-H	SA8	12.8
1229.2157	11632	1229.2204	M+Na	SA9	3.8
1251.1975	1672	1251.2023	M+2Na-H	SA9	3.8
1361.2483	7836	1361.2449	M+Na	SA10	2.5
1383.1200	1290	1383.2268	M+2Na-H	SA10	77.2

1493.2817	**4768**	**1493.2694**	**M+Na**	**SA11**	**8.3**
1515.1879	**1170**	**1515.2513**	**M+2Na-H**	**SA11**	**41.9**
1625.3221	**2639**	**1625.2939**	**M+Na**	**SA12**	**17.4**
1647.1940	**1287**	**1647.2758**	**M+2Na-H**	**SA12**	**49.7**
1757.3750	**1657**	**1757.3184**	**M+Na**	**SA13**	**32.2**
1779.2476	**930**	**1779.3004**	**M+2Na-H**	**SA13**	**29.7**
1889.4158	**1065**	**1889.3429**	**M+Na**	**SA14**	**38.6**
1911.2931	**659**	**1911.3249**	**M+2Na-H**	**SA14**	**16.6**
2021.4395	**662**	**2021.3674**	**M+Na**	**SA15**	**35.6**
2043.3311	**406**	**2043.3494**	**M+2Na-H**	**SA15**	**9.0**

Supplementary Table S5. Peak List for polyMA MALDI (Fig. S1); sodiated peaks.

Observed Mass (Da)	Intensity	Calc. Mass (amu)	Adduct	Polymer	Error (ppm)
497.2626	918	497.2721	M+Na	MA4	19.0
519.2581	580	519.2540	M+2Na-H	MA4	7.7
611.3363	3108	611.3402	M+Na	MA5	6.3
633.3119	2772	633.3221	M+2Na-H	MA5	16.2
725.3887	8249	725.4083	M+Na	MA6	27.0
747.3755	8615	747.3902	M+2Na-H	MA6	19.7
839.4567	16787	839.4763	M+Na	MA7	23.4
861.4373	16829	861.4583	M+2Na-H	MA7	24.4
953.5215	21831	953.5444	M+Na	MA8	24.0
975.5052	21367	975.5264	M+2Na-H	MA8	21.7
1067.5992	20991	1067.6125	M+Na	MA9	12.4
1089.5812	29611	1089.5944	M+2Na-H	MA9	12.2
1181.6714	17542	1181.6806	M+Na	MA10	7.8
1203.6570	32821	1203.6625	M+2Na-H	MA10	4.6
1295.7567	13957	1295.7487	M+Na	MA11	6.2
1317.7336	33357	1317.7306	M+2Na-H	MA11	2.3
1409.8358	9772	1409.8167	M+Na	MA12	13.6
1431.8053	25907	1431.7987	M+2Na-H	MA12	4.6

1523.9197	**7013**	**1523.8848**	**M+Na**	**MA13**	**22.9**
1545.8992	**22690**	**1545.8668**	**M+2Na-H**	**MA13**	**21.0**
1638.0011	**5056**	**1637.9529**	**M+Na**	**MA14**	**29.4**
1659.9788	**14871**	**1659.9348**	**M+2Na-H**	**MA14**	**26.5**
1752.0746	**2944**	**1752.0210**	**M+Na**	**MA15**	**30.6**
1774.0536	**9081**	**1774.0029**	**M+2Na-H**	**MA15**	**28.6**
1866.1465	**2013**	**1866.0891**	**M+Na**	**MA16**	**30.8**
1888.1432	**5056**	**1888.0710**	**M+2Na-H**	**MA16**	**38.2**
1980.2311	**1407**	**1980.1571**	**M+Na**	**MA17**	**37.3**
2002.2061	**2997**	**2002.1391**	**M+2Na-H**	**MA17**	**33.5**
2094.3154	**808**	**2094.2252**	**M+Na**	**MA18**	**43.1**
2116.2815	**2065**	**2116.2072**	**M+2Na-H**	**MA18**	**35.1**
2208.3928	**664**	**2208.2933**	**M+Na**	**MA19**	**45.1**
2230.3716	**1091**	**2230.2752**	**M+2Na-H**	**MA19**	**43.2**
2322.4685	**328**	**2322.3614**	**M+Na**	**MA20**	**46.1**
2344.4277	**753**	**2344.3433**	**M+2Na-H**	**MA20**	**36.0**
2436.5420	**234**	**2436.4295**	**M+Na**	**MA21**	**46.2**
2458.5156	**411**	**2458.4114**	**M+2Na-H**	**MA21**	**42.4**
2550.6003	**186**	**2550.4975**	**M+Na**	**MA22**	**40.3**
2572.5525	**302**	**2572.4795**	**M+2Na-H**	**MA22**	**28.4**

2664.6538	**156**	**2664.5656**	**M+Na**	**MA23**	**33.1**
2686.6287	**185**	**2686.5476**	**M+2Na-H**	**MA23**	**30.2**
2778.7061	**133**	**2778.6337**	**M+Na**	**MA24**	**26.0**
2800.6873	**120**	**2800.6156**	**M+2Na-H**	**MA24**	**25.6**
2914.7253	**124**	**2914.6837**	**M+2Na-H**	**MA25**	**14.3**

Supplementary Table S6. FRAP Kinetics of All Droplets Tested. FRAP curves were fit to the equation (see *Methods*) $I = I_0 + A*\exp(-t/\tau)$, where **I** = fluorescence intensity at time = t, $\mathbf{I_0}$ = intensity at time zero, t = time, A = a constant, and $\boldsymbol{\tau}$ = recovery time constant. $\mathbf{t_{1/2}}$, the half-time of recovery, was calculated as $\mathrm{Ln}(2)*\boldsymbol{\tau}$. In some cases, the recovery rate was too slow to properly fit the recovery curves. In those cases, the table entries are labeled as "SLOW". Highlighted samples in orange appear in Fig. 4 and Table 1 as representative data. Highlighted sample in green appears in Fig. S37 as representative data. SYBR = SYBR Gold, TfT = Thioflavin T, RNA = Hammerhead RNA (Sequence).

Sample	Dye	Diameter (µm)	I_0	A	τ (s)	R^2	$t_{½}$ (s)
All αHAs	SYBR	12.19	0.64601	-0.63362	892.52789	0.99758	618.6531905
All αHAs	SYBR	13.37	0.4176	-0.3999	669.58072	0.99445	464.1179882
All αHAs	SYBR	12.97	0.34492	-0.32582	415.28848	0.9835	287.856039
All αHAs	TfT	30.46	0.9758	-0.80986	646.4351	0.99171	448.074667
All αHAs	TfT	32.68	0.86543	-0.95974	707.01372	0.99348	490.0645666
All αHAs	TfT	35.18	0.97509	-0.7947	740.63818	0.99276	513.3712663
polyLA	SYBR	21.12	1.00914	-1.04627	102.800004	0.99627	71.25553293
polyLA	SYBR	13.13	0.98001	-0.99463	50.21695	0.99846	34.80773731
polyLA	SYBR	11.20	0.96521	-0.96092	45.67893	0.99766	31.66222154
polyLA	TfT	35.40	1.06627	-0.95099	82.86656	0.99863	57.43872243
polyLA	TfT	31.99	1.03423	-0.93057	71.94588	0.99636	49.86908387
polyLA	TfT	30.74	1.03574	-0.91121	62.05575	0.99685	43.01376815
polyPA	SYBR	10.80	SLOW	SLOW	SLOW	SLOW	SLOW
polyPA	SYBR	7.95	SLOW	SLOW	SLOW	SLOW	SLOW

polyPA	SYBR	17.79	SLOW	SLOW	SLOW	SLOW	SLOW
polyPA	TfT	23.65	0.3307	-0.27497	476.84824	0.99831	330.5260131
polyPA	TfT	11.46	0.57133	-0.53125	572.28484	0.99849	396.6776233
polyPA	TfT	9.55	0.75149	-0.69377	325.23486	0.99762	225.4356262
polySA	SYBR	6.62	SLOW	SLOW	SLOW	SLOW	SLOW
polySA	SYBR	8.50	SLOW	SLOW	SLOW	SLOW	SLOW
polySA	SYBR	4.98	SLOW	SLOW	SLOW	SLOW	SLOW
polySA	TfT	8.23	0.65775	0.62325	459.26942	0.9864	318.3413036
polySA	TfT	11.80	0.61653	-0.57984	301.13688	0.90281	208.7321793
polySA	TfT	11.70	1.37813	-1.33051	1017.07242	0.99545	704.9808803
polyMA	SYBR	21.87	SLOW	SLOW	SLOW	SLOW	SLOW
polyMA	SYBR	11.57	SLOW	SLOW	SLOW	SLOW	SLOW
polyMA	SYBR	12.85	SLOW	SLOW	SLOW	SLOW	SLOW
polyMA	TfT	26.45	0.66267	-0.50163	164.11544	0.97497	113.7561545
polyMA	TfT	34.50	0.52503	-0.30792	120.57836	0.95852	83.57855027
polyMA	TfT	23.24	0.74469	-0.58023	222.89682	0.98762	154.5003023
polyPA	RNA	9.00	0.61303	-0.277	641.5089	0.9849	444.6600853
polyPA	RNA	6.34	0.67438	-0.214	362.31786	0.91792	251.1396031

Supplementary Table S7. Swelling Assays. Mass of the gel sample (including the sample tube) before and after 72 hours of incubation in water followed by centrifugation and removal of water. polyLA appeared to decrease in mass following incubation in water (followed by removal), while the polyPA mass did change significantly. This could be due to the fact that in aqueous solution, some of the low mass species of polyLA may leach into the solution, which is further supported by two microscopy movies that track particle size after dilution in water (Supplementary Movies S1 and S2, and Figures S14 and S15). polyPA did not exhibit the same potential leaching phenomenon, but also did not clearly increase in mass, suggesting no significant swelling in these conditions.

Sample	Mass Before 72 Hr Incubation in Water and Subsequent Removal (mg)	Mass After 72 Hr Incubation in Water and Subsequent Removal (mg)	Difference in mass (mg)
polyLA	**925.0**	**913.5**	**-11.5**
polyLA	**920.1**	**909.4**	**-10.7**
polyLA	**919.8**	**909.2**	**-10.6**
polyPA	**919.3**	**918.2**	**-1.1**
polyPA	**922.4**	**921.3**	**-1.1**
polyPA	**923.2**	**922.5**	**-0.7**
Empty Tube	**905.2**	**904.3**	**-0.9**
Empty Tube	**910.1**	**909.1**	**-1.0**
Empty Tube	**911.8**	**910.4**	**-1.4**

Supplementary Movie S1. Movie tracking particle size of polyLA microdroplets (Fig. S14) after 1:10 dilution in water over time. Scale bar is 10 μm.

Supplementary Movie S2. Movie tracking particle size of a polyPA microdroplet, starred (Fig. S15) after 1:10 dilution in water over time. Scale bar is 100 μm.

Supplementary Movie S3. Movie of first hour after vortexing of a polyPA sample (same conditions as Fig. 2). There is no observable dissociation or coalescence. Scale bar is 100 μm.

Supplementary Movie S4. Movie of first hour after vortexing of a sample produced from all five αHAs (same conditions as Fig. 2). There is no observable dissociation or coalescence. Scale bar is 100 μm.

Supplementary Movie S5. Movie depicts between 1–1.5 hours after pH 8 introduction (800 mM Na-HEPES) to a sample containing all five αHAs (same conditions as Figs. 2 and S20). Scale bar is 100 μm.

Supplementary Movie S6. Movie depicts between 2–3 hours after pH 8 introduction (800 mM Na-HEPES) to a polyPA sample (same conditions as Figs. 2 and S21). Scale bar is 100 μm.

Supplementary Movie S7. Movie depicts the time between 0 and 60 minutes after vortexing of a polyPA sample (same conditions as Figs. 2 and S23). Scale bar is 10 μm.

Supplementary Movie S8. Movie depicts rapid coalescence of droplets within 30 minutes of a polyPA sample in 100 mM NaCl (same conditions as Figs. 2 and S23). Scale bar is 10 μm.

Supplementary Movie S9. Movie depicts rapid coalescence of droplets within 20 minutes of a polyPA sample in 100 mM Na-HEPES pH 8 (same conditions as Figs. 2 and S23). Scale bar is 10 μm.

Supplementary Movie S10. FRAP Recovery of polyLA droplet with 20 mM TfT dye from Fig. 4a (31.99 μm). Scale bar is 100 μm.

Supplementary Movie S11. FRAP Recovery of polySA droplet with 1X SYBR Gold dye from Fig. 4b (8.50 μm). Scale bar is 100 μm.

Supplementary Movie S12. FRAP Recovery of polyPA droplet with 10μM Hammerhead RNA from Fig. S37 (9.00 μm). Scale bar is 100 μm.

References

1. Iqbal M, et al. (2016) Aqueous two-phase system (ATPS): an overview and advances in its applications. *Biol Proced Online* 18:18.

2. Atefi E, Fyffe D, Kaylan KB, Tavana H (2016) Characterization of Aqueous Two-Phase Systems from Volume and Density Measurements. *J Chem Eng Data* 61(4):1531–1539.

3. Priftis D, Tirrell M (2012) Phase behaviour and complex coacervation of aqueous polypeptide solutions. *Soft Matter* 8(36):9396–9405.

4. Aumiller WM Jr, Pir Cakmak F, Davis BW, Keating CD (2016) RNA-Based Coacervates as a Model for Membraneless Organelles: Formation, Properties, and Interfacial Liposome Assembly. *Langmuir* 32(39):10042–10053.

5. Koga S, Williams DS, Perriman AW, Mann S (2011) Peptide-nucleotide microdroplets as a step towards a membrane-free protocell model. *Nat Chem* 3(9):720–724.

6. Apel CL, Deamer DW, Mautner MN (2002) Self-assembled vesicles of monocarboxylic acids and alcohols: conditions for stability and for the encapsulation of biopolymers. *Biochimica et Biophysica Acta (BBA) - Biomembranes* 1559(1):1–9.

7. Mansy SS, Szostak JW (2008) Thermostability of model protocell membranes. *Proc Natl Acad Sci U S A* 105(36):13351–13355.

8. Thibon L, Lorenzo LE, Piché M, De Koninck Y (2017) Resolution enhancement in confocal microscopy using Bessel-Gauss beams. *Opt Express* 25(3):2162–2177.

9. Zangi R, Hagen M, Berne BJ (2007) Effect of ions on the hydrophobic interaction between two plates. *J Am Chem Soc* 129(15):4678–4686.

10. Xue C, Lin TY, Chang D, Guo Z (2017) Thioflavin T as an amyloid dye: fibril quantification, optimal concentration and effect on aggregation. *R Soc Open Sci* 4(1):160696.

11. Tuma RS, et al. (1999) Characterization of SYBR Gold nucleic acid gel stain: a dye optimized for use with 300-nm ultraviolet transilluminators. *Anal Biochem* 268(2):278–288.

12. Melikishvili M, Rodgers DW, Fried MG (2011) 6-Carboxyfluorescein and structurally similar molecules inhibit DNA binding and repair by O^6-alkylguanine DNA alkyltransferase. *DNA Repair* 10(12):1193–1202.